Mechanisms for minimizing height-related stomatal conductance declines in tall vines

Domec, Jean-Christophe

2019-11

Domec , J-C , Berghoff , H , Way , D , Moshelion , M , Palmroth , S , Kets , K , Huang , C-W & Oren , R 2019 , ' Mechanisms for minimizing height-related stomatal conductance declines in tall vines ' , Plant, Cell and Environment , vol. 42 , no. 11 , pp. 3121-3139 . https://doi.org/10.1111/pce.13593

http://hdl.handle.net/10138/315196
https://doi.org/10.1111/pce.13593

unspecified
acceptedVersion

Domec Jean-Christophe (Orcid ID: 0000-0003-0478-2559)
Way Danielle (Orcid ID: 0000-0003-4801-5319)

Mechanisms for minimizing height-related stomatal conductance declines in tall vines

Running Title: Full structural & hydraulic compensation in kudzu

Jean-Christophe Domec[1,2,8], Henry Berghoff[2,9], Danielle Way [2,3,10], Menachem Moshelion[4,11], Sari Palmroth[2,12] Katre Kets[5,13], Cheng-Wei Huang[6,14] Ram Oren[2,7,14]

[1] Bordeaux Sciences Agro, INRA UMR 1391 ISPA, F-33170 Gradignan, France
[2] Nicholas School of the Environment, Duke University, Durham, NC 27708, USA
[3] Department of Biology, Western University, London, ON, Canada
[4] The R.H. Smith Institute of Plant Sciences and Genetics in Agriculture, The R.H. Smith Faculty of Agriculture, Food and Environment, The Hebrew University of Jerusalem, Rehovot 76100, Israel
[5] Institute of Botany and Ecology, University of Tartu, Lai 40, 51005 Tartu, Estonia
[6] Department of Biology, University of New Mexico, Albuquerque, NM 87131, USA
[7] Department of Forest Sciences, University of Helsinki, Helsinki, FI-00014, Finland

[8] jc.domec@agro-bordeaux.fr
[9] berghoffhg@gmail.com
[10] dway4@uwo.ca
[11] menachem.moshelion@mail.huji.ac.il
[12] sari.palmroth@duke.edu
[13] katre.kets@gmail.com
[14] ch224@unm.edu
[15] ramoren@duke.edu

This article has been accepted for publication and undergone full peer review but has not been through the copyediting, typesetting, pagination and proofreading process which may lead to differences between this version and the Version of Record. Please cite this article as doi: 10.1111/pce.13593

Abstract

The ability to transport water through tall stems hydraulically limits stomatal conductance (g_s), thereby constraining photosynthesis and growth. However, some plants are able to minimize this height-related decrease in g_s, regardless of path length. We hypothesized that kudzu (*Pueraria lobata*) prevents strong declines in g_s with height through appreciable structural and hydraulic compensative alterations. We observed only a 12% decline in maximum g_s along 15 m long stems, and were able to model this empirical trend. Increasing resistance with transport distance was not compensated by increasing sapwood-to-leaf-area ratio. Compensating for increasing leaf area by adjusting the driving force would require water potential reaching -1.9 MPa, far below the wilting point (-1.2 MPa). The negative effect of stem length was compensated for by decreasing petiole hydraulic resistance, and by increasing stem sapwood area and water storage, with capacitive discharge representing 8%-12% of the water flux. In addition, large lateral (petiole, leaves) relative to axial hydraulic resistance helped improve water flow distribution to top leaves. These results indicate that g_s of distal leaves can be similar to that of basal leaves, provided that resistance is highest in petioles, and sufficient amounts of water storage can be used to subsidize the transpiration stream.

Summary Statement

Fast-growing vines such as kudzu must supply all leaves with sufficient water to maintain high photosynthetic and growth rates. We found no physiological difference in vine growing in any orientation but were able to identify the main structural and functional mechanisms supporting a nearly uniform supply of water along the stem, with large lateral relative to axial hydraulic resistance helping even water flow distribution with height.

Key words: capacitance, Electrical Circuit Analogy, hydraulic compensation, hydraulic resistance, lianas, long-distance transport, *Pueraria lobata*

Introduction

Simple models of water flow from soil to leaves assume that water uptake balances water lost in transpiration. Further simplifications assume average hydraulic conductance between two points, one in the soil and another in the crown, defining the two end points for the water potential difference driving water flow from the soil to leaves (Whitehead 1998). Models based on these assumptions have been successfully used to describe variation in stomatal conductance (g_s) at scales ranging from tree crowns to forest stands (Mencuccini et al., 1997; Schäfer et al., 2000; McDowell et al., 2002; Ambrose et al., 2010).

However, xylem hydraulic conductance varies by organ (Ewers & Zimmermann 1984; Andrade et al., 1998; Domec et al., 2012), and conductance in each plant organ may respond differently to changes in water potential (Tsuda & Tyree 1997; Johnson et al., 2016). Moreover, capacitive discharge of stored water within the hydraulic pathway itself is important for buffering transpiration-induced fluctuations in water potential (Meinzer et al., 2008; Huang et al., 2017). Hydraulic conductance of the soil (Running 1980) and the xylem pathway (Venturas et al., 2017) both decrease as water potential declines. Thus, coarse attributes (e.g., averages of path length from soil to leaves, root or sapwood area per unit of leaf area, and predawn to daytime leaf water potential gradients) may work reasonably well in capturing the variability of transport capacity to the average leaf among individuals, stands, and ecosystems, but only if these attributes dominate over more nuanced sources of variation. One may therefore ask: what are the limits within which simple hydraulic approximations are useful for describing the variation of g_s within plants? To answer this question, it is necessary to account for the relative contribution of each plant organ to the total resistance and capacitance to water flow.

Vines preferentially allocate carbon to leaves to take advantage of their position in the forest canopy (Carter & Teramura, 1988), while simultaneously shading competitors (Sasek & Strain, 1989). Canopies of vine species that are shade- and freeze-intolerant die back each year, and thus must regrow quickly each spring to overtop nearby vegetation. In self-supported plants, hydraulic adjustments do not fully compensate for the size-related decline in water transport and thus g_s of tall trees (Schäfer et al., 2000; Ryan et al., 2006). However, to maintain high photosynthetic rates and provide a local source of carbohydrates for extension growth, vines must maintain high g_s for which large quantities of water must be transported to the tops of tall canopies (Clearwater et al., 2004; Johnson et al., 2013). Yet, compared to trees, vines have a much lower sapwood area per unit of leaf area, which in trees

has been associated with reduced water supply and carbon assimilation per leaf area (Whitehead et al., 1984; Phillips et al., 2003; Ewers et al., 2007). Furthermore, compared with trees, the flow path along the stem of vines is much longer relative to the conducting stem cross-sectional area (Rosell & Olsen 2014; Filartiga et al., 2014). Despite those restrictions to maximum water flow rates through long and narrow stems, vines can contribute a significant proportion of total evapotranspiration and carbon uptake in ecosystems (Restom & Nepstad, 2001). This implies that vines must have mechanisms compensating for hydraulic limitations, imposed by extended path-length and increased leaf size with height (Figure 1). Proposed mechanisms for increasing hydraulic flow in vine species include deeper rooting systems (Chen et al., 2015), increased stem hydraulic conductivity and water storage (Gartner 1991; Johnson et al., 2013), increased size and number of vessels (Masrahi 2014; Rosell & Olsen, 2014), and segmentation of hydraulic resistance (Taneda & Tateno, 2011).

Even in the absence of any hydraulic limitation related to path length, vine height might affect turgor and leaf water potentials through gravity (Woodruff et al. 2004). One way to disentangle the effect of gravity on tissue structure and function is to train vines or trees to grow at different angles. This would allow distinguishing between the effect of path length alone (e.g., in horizontally growing stems) from that of the joint path length and gravity.

There are several models that can account for the different and variable resistances along the water transport pathway, based on an Ohm's law analogy, Darcy's flow, or porous media formulations (Edwards et al., 1986; Williams et al., 1996; Bohrer et al., 2005; Ewers et al., 2007). The formal hydraulic model of Whitehead et al. (1984) predicts that a water homeostasis must exist between transport capacity and transpirational loss, such that full hydraulic compensation can prevail if this is advantageous to the plant. Using an Ohm's law analogy, Taneda & Tateno (2011) modeled that a large lateral relative to axial resistance to flow is responsible for an even flow distribution to leaves along horizontally growing stems of the kudzu vine *Pueraria lobata* (Wild.). However, the model may not match the behavior of stems growing vertically on trees because of increased leaf size with height, and because tissues developing under more negative water potentials trade-off conductivity for safety. These tissues may develop such that their vulnerability to embolism and loss of hydraulic function is lower, but so is their hydraulic conductivity (Schubert et al., 1999; Sperry et al., 2002; Tombesi et al., 2014).

The aim of this study was to investigate the mechanisms underlying the ability to efficiently distribute water along stems at a great distance from the soil while maintaining

high gas exchange rates. To accomplish this, we used kudzu as a model system. Kudzu is a perennial liana native to East Asia that was introduced as a forage crop in the south-eastern USA, and has since spread into adjacent forests and grassland (ISSG 2013, Figure S1). We compared field values of hydraulic resistance and g_s along the water transport pathway to values modeled using the Ohm's electrical analogy applied to a hydraulic circuit. We specifically examined hydraulic traits and gas exchange rates of kudzu plants grown in full sun at various angles, thus allowing some degree of separation between the path length and the height water traveled from the soil surface, which affects the driving force, resistance and potentially causes hydraulic adjustments (Magnani et al., 2000). As depicted in Figure 1, we hypothesized that: 1) vines growing vertically, in an ecologically realistic manner, would show greater lateral relative to axial resistance than vines growing horizontally; 2) vines growing at steeper angles would have hydraulic traits that help mitigate potential height-driven declines in g_s, compared to horizontally grown stems, specifically: 2a) lower leaf water potentials for a given path length, to drive a greater difference in water potential between leaves and soil; 2b) a larger difference between stem and petiole resistance; and 2c) larger tissue capacitance with height, to shift the diurnal reliance of transpiration from root uptake of soil water (increasingly difficult to access with distance) to more easily accessible water stored near the sites of transpiration.

To evaluate the relative contribution of each compensating mechanism for maintaining g_s with distance from the soil, regardless of stem orientation, we employed a model (Taneda & Tateno, 2011) modified to account for the utilization of water stored along the stem, and for the loss of stem hydraulic capacity due to cavitation-induced embolism. We hypothesize that, contrary to previously described behavior of self-supported plants (McDowell et al., 2002; Ryan et al., 2006), appreciable structural and hydraulic compensative alterations are necessary to allow sufficient water delivery to kudzu leaves, thus supporting high gas exchange rates along the entire stem (Figure 1).

Theory

The Hydraulic Limitation Hypothesis (HLH) predicts that taller individuals have lower gas exchange rates, reflecting the effect of gravity and path-length on liquid water transport (Ryan & Yoder, 1997). The effects of increasing height include an increased flow resistance with path length (L_{path}), and a decreasing water potential gradient driving the flow from soil to leaf ($\Delta\Psi$), as the counter force of hydrostatic pressure increases with the height of the

water column (notations and units are listed in Table 1). A simplified representation of leaf conductance to water vapor (g_l) based on a Darcy's law analogy is (Whitehead et al., 1984; Whitehead & Hinckley, 1991; McDowell et al., 2002):

$$g_{\mathrm{l}} = \frac{k_{\mathrm{s}} * \Delta\Psi * \mathrm{sapwood\_area} * \Omega\,(T_{air})}{L_{\mathrm{path}} * \mathrm{leaf\_area} * \mathrm{VPD}} \quad (1),$$

where g_l accounts for the combined effects of g_s and the boundary layer conductance (g_{bl}) on water loss through transpiration, k_s is the "whole"-xylem specific hydraulic conductivity, VPD is the vapor pressure deficit, and □ is a coefficient that fluctuates with air temperature (T_{air}) based on changes in the psychometric constant, latent heat of vaporization, specific heat of air at constant pressure, and the density of air (Ewers et al., 2001). Hereafter we refer to Equation 1 as the Simplified Hydraulic Formulation (SHF). Boundary layer conductance is mainly determined by the characteristic dimension of the leaf (L_{leaf}) and wind velocity (u; taken as 4.2 m s^{-1} in our simulations, which represented the daily mean value during our measuring period) through forced convection (Huang et al., 2015; Stokes et al., 2006), and can be estimated as (Forseth & Teramura, 1987; Jones, 1992):

$$g_{\mathrm{bl}} = 304\sqrt{\frac{u}{L_{leaf}}} \quad (2).$$

According to SHF, and consistent with HLH, L_{path} increases with height, limiting g_s and thus g_l of upper leaves (Pennisi, 2005). Not only does increasing height (and L_{path}), increase resistance to water flow, it also reduces $\Delta\Psi$ since (Zimmermann, 1983; Schäfer et al., 2000; Domec et al., 2008):

$$\Delta\Psi = \Psi_{soil} - \Psi_{leaf} - \rho_w G h \cong \Psi_{soil} - \Psi_{leaf} - 0.01h \quad (3),$$

where Ψ_{soil} is the soil water potential, Ψ_{leaf} is the leaf water potential, ρ_w is the density of water, G is the acceleration of gravity, and h is the mid-crown height above the ground, or the height of the leaf of which Ψ_{leaf} represents the crown or canopy. The SHF can explain variation of g_s among trees of different heights in a given stand (Schäfer et al., 2000; Ambrose et al., 2010), between undisturbed crowns and those of reduced mid-crown height following fire-induced epicormic branching (Nolan et al., 2014), between shorter, young and taller, old stands (Ryan et al., 2000; Phillips et al., 2003), and among ecosystems (Novick et al., 2009).

Nevertheless, given the simplifications inherent in the SHF, it is not likely to perform well when average hydrological properties are used to describe wide distributions of these properties, especially for properties that are non-linearly related to g_s. In such cases, the behavior of the system computed based on the average of a property (such as k_s) will not

equal the average of the behavior computed from the distribution of the property. Furthermore, SHF cannot be readily implemented to produce a distribution of within-plant variation of g_s. Instead, building on Ohm's Law, the flow of water through a stem with leaves distributed along its length (such as a vine) can be approximated as an electrical circuit with resistors in parallel (Van den Honert, 1948; Taneda & Tateno, 2007).

In order to determine flow through each node (i.e. petiole or leaf), Taneda and Tateno (2011) employ Kirchhoff's Voltage Law under steady state (i.e. without movement of water between the transpirational path and tissue water sources):

$$E_k = \sum_{i=k}^{N}(I_{Axial,i} * R_{Axial.i}) + \left(I_{Lateral,k} * R_{Lateral,k}\right), \quad (4),$$

where k is the node number with k=1 as the most distal node and k=N (i.e. N is the total number of nodes) as the most basal node, E_k is the driving force for flow at kth node, $I_{Axial,k}$ and $R_{Axial,k}$ are respectively the flow and the resistance through the axial portion between kth node and (k+1)th node, and $I_{Lateral,k}$ and $R_{Lateral,k}$ are, respectively, the flow and the resistance through the lateral portion at kth node. Moreover, the axial flow rate at the kth node can be defined as the sum of the lateral flow rates distal to that node according to Kirchhoff's current law:

$$I_{Axial,k} = \sum_{i=1}^{k} I_{Lateral,i} \quad (5).$$

To run this Distributed Hydraulic Formulation (DHF) model, we solve Equation (4) for lateral flow rate at each node simultaneously ($I_{Lateral,k}$). For axial resistance, we use the specific resistance in the stem between two nodes, R_{stem}, defined as:

$$R_{\text{stem}} = \frac{L_{\text{internode}}}{k_{\text{s\_stem}} * X_{\text{stem}}} \quad (6),$$

where $L_{\text{internode}}$ is internode length, $k_{\text{s\_stem}}$ is the stem hydraulic conductivity on a sapwood area-basis, and X_{stem} is the stem cross-sectional area. In the model, the increase in stem embolism with increasing stem pressure was taken into account by relating R_{stem} to vulnerability to embolism from measured vulnerability curves. For lateral resistance, we sum the specific petiole and leaf resistances at each location. Petiole resistance, R_{petiole}, is defined as:

$$R_{\text{petiole}} = \frac{L_{\text{petiole}}}{k_{\text{s\_petiole}} * X_{\text{petiole}}} \quad (7),$$

where L_{petiole} is the petiole length, $k_{\text{s\_petiole}}$ is the petiole conductivity, and X_{petiole} is the petiole cross-sectional area. Leaf resistance, R_{leaf}, is defined as:

$$R_{\text{leaf}} = \frac{1}{K_{\text{leaf}} * \text{leaf\_area}} \quad (8),$$

where K_{leaf} is the leaf specific conductance. For E_k, we use measured $\Delta\Psi$ at each node. I_{Axial} is defined by Equation (5), leaving $I_{Lateral}$ as the only unknown in the complete set of equations.

Summed for an entire plant, the water supply used in transpiration may be greater than the amount of water taken up at the same time from the soil because of the use of stored water. Plant utilization of water stored in their tissues can contribute a significant fraction of overall water loss, especially in lianas made of soft and elastic tissues (Scholz et al., 2011; Pratt & Jacobsen, 2017). Water storage capacity (capacitance) can be defined as the amount of water withdrawn from a given volume or area of a plant tissue per $\Delta\Psi$. After measuring leaf (C_{leaf}), petiole ($C_{petiole}$) and stem (C_{stem}) capacitances (see Methods below), these were converted into a storage flux through the axial (S_{Axial}) and lateral ($S_{Lateral}$) portion at the k^{th} node by multiplying them by leaf or stem water potentials. We assumed that total capacitive discharge occurred over a 3- or 6-hour period, which corresponded to either a fast of slow rate of daily withdrawal from storage (Scholz et al. 2011). The calculated total water flow at the k^{th} node became:

$$F_{Lateral,k} = I_{Lateral,k} + S_{Axial,k} + S_{Lateral,k} \quad (9).$$

To relate flow to g_l and then g_s, we apply:

$$g_{l,k} = \frac{F_{Lateral,k} * \Omega(T_{air})}{\text{leaf\_area} * \text{VPD}} \quad (10), \text{ and}$$

$$g_{s,k} = \frac{g_{l,k} * g_{bl,k}}{g_{l,k} - g_{bl,k}} \quad (11).$$

Methods

Setting

The experiment was established in a field located in the Duke Forest (Durham County, USA: 36.01 °N, 79.00 °W) where the long term mean annual temperature and precipitation are 15.5 °C and 1145±180 mm (mean ± standard deviation), respectively. The soil is mostly clay to a depth of 1-1.5 m. Kudzu seeds were first grown individually in pots at the Duke University Phytotron in June 2010, and the pots were moved outside in early July 2010. In June 2011, the aboveground biomass was trimmed back to increase the root-to-shoot ratio just prior to planting in the soil at the study site. Plants were planted into the soil at the field site in June 2011 and irrigated to avoid water limitations, averaging three times per week during the growing season of 2011, to ensure vigorous establishment. During the 2012 growing season, plants were watered at least every other day except on rainy days.

To study leaf traits along a height and length gradient, a 15-m tall tower was erected at the center of the field, with twelve 15-m long wires attached at four different angles (horizontal 0°, 30°, 60°, and vertical 90°), between the tower and each of twelve anchor points on the ground (Figure S1). One kudzu seedling was planted at the anchor point of each wire (3 replicates x 4 angles = 12 plants). To compare horizontal stems to angled ones within the same plant in addition to between plants, each plant was trained to grow multiple shoots along the ground at 0° and around a wire at one of the four treatment angles. Both heights and path lengths of each measured leaf were determined from the soil surface. Browsing by deer affected early season growth in 2012, and may have contributed to different growth patterns among individuals. Deer were prevented from browsing once this was recognized.

To expand our dataset and compare structural and hydraulic parameters to vines growing in their natural habitat, in September 2016, we also collected six entire kudzu plants that were climbing on trees (Durham County, NC, USA).

Gas Exchange

On September 7-9, 2012, gas exchange was measured on the middle leaflet of 54 leaves (20 at 90□, 9 at 60°, 4 at 30°, 21 at 0□) using a LI-6400 portable photosynthesis system (Li-Cor, Lincoln, NE, USA). For each leaf, the chamber was set to match prevailing environmental conditions assessed immediately prior to the measurement: atmospheric CO_2 concentration (376-413 ppm), relative humidity (26-61 %), photosynthetically active radiation (PAR; 300-2000 μmol m^{-2} s^{-1}), and leaf temperature (27-35 °C). Water potentials were measured immediately afterwards, as described below. All gas exchange results were expressed on a leaf area basis. Because the g_s of individual leaves in field settings is often limited by irradiance on leaf surfaces (Niinemets, 2010), rather than hydraulically controlled, we utilized a data reduction approach to account for the effects of changing PAR and vapor pressure deficit (VPD) on measured g_s before assessing hydraulic controls of g_s (Tor-ngern et al., 2015). Specifically, we first calculated the sensitivity of g_s to ln(VPD) (the parameter b of the regression fit $g_s = g_{s\text{-}ref} - b * \ln(VPD)$) that is expected to increase with the reference conductance (g_{s-ref}), i.e. g_s at VPD=1kPa (Oren et al., 1999). Then, to account for variation of g_s caused by VPD and PAR, we (i) calculated the residual of each value from its respective fit representing a PAR range, and (ii) added the value to the $g_{s\text{-}ref}$ obtained from the same fit, thus normalizing all g_s values to their expected values at a VPD of 1 kPa, i.e., to expected $g_{s\text{-}ref}$ (here referred to as $g_{s\text{-}ref}'$). Following, we related these $g_{s\text{-}ref}'$ values to the actual PAR in

which each original g_s value was measured, obtaining a relationship that allowed us to estimate the average maximum $g_{s\text{-}ref}'$. Taking the residuals of this fit, and adding them to the fitted maximum $g_{s\text{-}ref}'$ we obtained a maximum g_s normalized to 1 kPa VPD and maximum PAR ($g_{s\text{-}ref}'m$).

On September 10-13, 2012, photosynthetic capacity was measured on 24 leaves grown at the top (n=15) and the base of the 90□ plants (n=9). Net CO_2 assimilation rates (A_{net}) versus intercellular CO_2 concentrations were measured at 30 °C leaf temperature, 50±10 % relative humidity and 1500 μmol m^{-2} s^{-1} PAR. The chamber CO_2 concentrations were set to ambient and sequentially lowered to 50 ppm. These data were used to estimate the maximum Rubisco carboxylation rate (V_{cmax}), according to Farquhar et al. (1980).

Water Potential

Along with the gas exchange measurements, Ψ_{leaf} was measured using a pressure chamber (PMS Ins., Albany, OR, USA) every 3 m along both the height and length gradients of one wire of each treatment angle, for four plants each day of the first three-day campaign. To assess maximum (least negative) Ψ_{leaf}, one leaf at each location was sampled at pre-dawn. After the predawn sample was excised, a second adjacent leaf at each location was wrapped in an aluminum foil-covered plastic bag to obtain Ψ_{stem}, corresponding to the leaf water potential in equilibrium with the water potential of the stem (Richter et al., 1997). Between 8:30 and 11:00 each day, Ψ_{stem} was measured on these non-transpiring covered leaves, and Ψ_{leaf} was assessed on a third, freely transpiring leaf next to the Ψ_{stem} leaf at each location. The third leaf was excised immediately following measurement of its gas exchange rates. Altogether, three leaves at each of 54 locations at ~3 m intervals along the stems were sampled for Ψ_{leaf} (162 leaves total).

Following the approach used to determine, and account for, the effects of changing PAR and VPD on measured g_s, we accounted for the effect of these two variables on the Ψ_{leaf} of transpiring leaves. To do so, we first calculated the residual of the decline in Ψ_{leaf} and Ψ_{stem} with VPD for a given PAR range. We then added the value to the Ψ_{leaf} and Ψ_{stem} obtained from the same fit, thus normalizing all Ψ_{leaf} and Ψ_{stem} values to their expected values at a VPD of 1 kPa ($\Psi_{leaf\text{-}ref}$).

From September 24 to October 4, 2012, 20 leaves at the tip and base of the 90° and 0° treatment angles were sampled for pressure-volume measurements. Leaves were sampled at predawn and transported to the lab in plastic bags, keeping the cut end of the petiole

submerged in water. For at least one hour prior to measurement, leaves were allowed to absorb water and rehydrate in open air at 25 °C while petioles were kept in water. Leaf mass and Ψ_{leaf} were then repeatedly measured as leaves dried on a laboratory bench. At least five points were measured before the turgor loss point, and at least six points after it, thus accurately approximating the linear portion of the relation between the inverse of leaf water potential and leaf relative water content (RWC, %). The curves were created by plotting the inverse of Ψ_{leaf} against RWC until values of Ψ_{leaf} neared -4.0 MPa. Following pressure-volume measurement, leaves were dried at 80 °C. Osmotic potential at full turgor ($\Psi_{\pi 100}$), water potential at leaf turgor loss point (Ψ_{TLP}) and C_{leaf} were estimated from pressure-volume curves (Tyree & Hammel, 1972). The Ψ_{leaf} corresponding to turgor loss was estimated as the point where the plot of $1/\Psi_{leaf}$ vs RWC becomes linear. The slope of the quasi-linear relationship prior to, and following turgor-loss provided C_{leaf} for pre-turgor and post-turgor loss, respectively. The osmotic potential at full turgor was taken as the y-intercept of a line fitted to the post-turgor loss data for the plot of $1/\Psi_{leaf}$ versus 100-RWC. The bulk tissue modulus of elasticity (ε) was estimated as the slope of the relationship between turgor pressure (the difference between the osmotic potential line fitted to the post-turgor loss data as above and the water potential curve) and RWC (as in Meinzer et al., 2008).

Hydraulic Conductivity

Liquid-phase resistances to water transport aboveground were estimated from specific hydraulic conductivity of stems, petioles, and leaves along the height and length gradients. Stem samples, roughly 1.8 m long, taken from the base and tip of each of the three vines grown at 0°, 30°, 60° and 90° angles, were transported to the lab, keeping the cut ends submerged in water. Estimates of longest vessel length were made using the compressed-air method of Ewers and Fisher (1989), whereby air is forced into the proximal end of the segment at 75 kPa and the distal end is submerged in water. Stem segments of 5 cm were cut from the distal end until air bubbles were seen, and the final length of the segment was then taken as the longest vessel length. Before hydraulic measurements, stem segments that were at least 50% longer than the mean vessel length (0.76±0.27 m) were recut at both ends underwater, stripped of leaves and flushed at 0.2 MPa with filtered (0.22 μm), and vacuum-degassed deionized water for at least 15 min to refill embolized vessels (Melcher et al., 2012). Note that more than 80% of the samples used for stem hydraulics were twice as long as the mean vessel length. At each end of the stem, the xylem was exposed by removing the

thin tissue surrounding it and attached to a tubing system suffused with filtered, deionized water. At the proximal end of the stem, 0.005 MPa of pressure was applied, and efflux was measured at the distal end with a 1 mL graduated pipette. Water temperature was measured before and after each measurement to account for changes in the viscosity of water and the data were normalized to 20 °C. Stem specific conductivity (k_{s_stem}) was calculated as the mass flow rate of the perfusion solution divided by the pressure gradient across the segment, normalized by the xylem cross-sectional area and length (Domec et al., 2012).

Additionally, to determine the upper limit of k_{s_stem}, the theoretical specific conductivity (k_{s_theo}), which represents the open vessel conductivity (Sperry et al., 2005), was calculated according to the equation for capillaries (Calkin et al.,1986):

$$k_{s\_theo} = \frac{n\pi\rho D_h^4}{128 X_{stem}} \quad (12)$$

where n is the number of vessels, ρ is density of water (kg m^{-3}), □ is dynamic viscosity of water (MPa s) and D_h is the hydraulically weighted vessel diameter (m) calculated as:

$$D_h = \left[\frac{\sum_{i=1}^{n} d_i^4}{n}\right]^{1/4} \quad (13),$$

where d_i is the diameter of the i^{th} vessel summed over the number of vessels, n. Vessel lumen diameter was determined from hand-made sections of each of the three 90° plants used for k_{s_stem} and vulnerability to embolism curves. One sample per vine was taken from the top section (12-14.5 m), one from the mid section (6-8 m), and one from the base. In addition, one extra sample was taken from the top and bottom of one of the vines, for a total of 11 samples. Sections were mounted and viewed using a MU300-CK digital camera fixed to an Amscope phase contrast trinocular microscope (AMSCOPE, Irvin, CA, USA) connected to a PC using Metavue software (Universal Imaging Corp., Downington, PA, USA). Images were analyzed using the freeware software ImageJ (NIH, USA, **http://rsb.info**. nih.gov/ij/). Anatomical sections were also used to calculate the fraction of parenchyma tissue over the whole cross section.

Stem vulnerability to embolism curves were constructed using the air-injection method (Sperry & Saliendra, 1994). Reliable measurements of hydraulic vulnerability can be obtained with this method, especially when using a small pressure sleeve (Ennajeh et al., 2011). After the maximum conductivity was measured (maximum k_{s_stem}), stems were placed in a double-ended pressure sleeve (13 cm in length) and pressurized for 1 min. The stem was then removed from the pressure sleeve and variables necessary to estimate k_{s_stem} were

measured again as described above, except that the hydraulic pressure head was adjusted to less than 0.004 MPa to avoid refilling embolized vessels. Pressure was applied at increments of 0.5 MPa between consecutive k_{s_stem} estimates until k_{s_stem} dropped to 10% or less of maximum k_{s_stem}.

Variation in $k_{s\_petiole}$ with stem length and height was measured on the 162 petioles of the leaves on which Ψ_{leaf} and Ψ_{stem} was determined in the field. After being excised, leaves were transported to the lab in plastic bags and kept in the refrigerator for a maximum of three days. Petioles were cut from each leaf and flushed with filtered, deionized water to remove embolisms prior to measuring $k_{s\_petiole}$ using a high-pressure flow meter (HPFM, Dynamax Inc., Houston, TX, USA) as described in Tsuga and Tyree (1997) and Melcher et al. (2012).

Whole-leaf hydraulic conductance (K_{leaf}) was calculated as (Meinzer, 2002):

$$K_{leaf} = \nu/\nu_o \, E/(\Psi_{stem} - \Psi_{leaf}) \quad (14),$$

where ν and ν_o are respectively the kinematic viscosities of water at the measured leaf temperature and at 20 ºC and E is the transpiration rate (mol m^{-2} s^{-1}) measured in the field with the LI-6400 portable photosynthesis system.

Water storage

Small pieces (approximately 1.5 cm in length) of stem and petiole representing the range of diameters of the samples used for hydraulic measurements were used to construct xylem moisture release curves for estimating capacitance (Meinzer et al., 2008). One stem and one petiole sample were measured from the top and the bottom of the six extra vertical vines sampled in September 2016 (n=12 for stems and petiole). The samples were vacuum-infiltrated overnight in water. The saturated samples were then blotted on a paper towel to remove excess water, weighed, and placed in a Wescor C-30 sample chamber fitted with a PST-55-15 thermocouple psychrometer (Wescor Equipment Inc., Logan, UT, USA). These chambers were then submerged in a cooler of water for 3–6 h to allow the sample to equilibrate with the chamber air. After the equilibration period, the millivolt readings were recorded using an eight-channel water potential datalogger (PsΨchro, Wescor Equipment Inc., Logan, UT) connected to a computer. Following the measurement, the samples were removed from the chambers, weighed, and allowed to dry on the laboratory bench for approximately 15 minutes before repeating the process (except for the saturation step). Samples were then dried for 48 hours before the dry mass was weighed. The millivolt output of the psychrometer was converted to MPa based on calibration curves from salt solutions of

known water potentials. Samples were measured repeatedly until water potential values reached approximately −4 MPa for stems. For the petioles, water potentials lower than -2.5 MPa were not possible to reach probably because not enough water vapor could equilibrate in the chamber once the samples had lost a significant amount of water. Moisture release curves were determined by plotting the cumulative mass of water lost versus the xylem water potential, and the capacitances of the stem (C_{stem}) and petiole ($C_{petiole}$) were estimated by plotting a regression to the initial, nearly linear, phase of the plot until Ψ_{TLP}, which encompassed the physiological operating range of stem water potential (Meinzer et al., 2008). Usually $C_{petiole}$ and C_{stem} are represented on a volume basis (kg m^{-3} MPa^{-1}), therefore, the conversion was done by multiplying the capacitance values by tissue volume. In leaves, capacitive water on a leaf area basis was directly calculated from pressure volume curves as described above.

Plant Structure

For each Ψ_{leaf} sample, leaf area was measured after petioles were removed using a leaf area meter (LI-3100, Li-Cor, Lincoln, NE). Leaf area measurements are slight overestimates (<3%) because the petiolules (< 5 cm^2) connecting leaflets to the petiole were not removed. Leaves were then dried at 65 °C for 48 h and weighed.

After performing vulnerability curve assessments for each stem sample, sapwood diameter was measured using a caliper and directly converted to X_{stem} because of the thin phloem tissue and the absence of pith. The distance between each leaf ($L_{internode}$) was measured to estimate the distance for water flow between leaves as well as the number of leaves per stem. Stems were tightly coiled around the training wires, resulting in a three-dimensional shape after sampling. Thus, despite stretching, measured $L_{internode}$ may be slightly underestimated. Petiole diameter was measured with a digital caliper prior to $k_{s\_petiole}$ assessment and converted to $X_{petiole}$. Stem and petiole tissue densities (g cm^{-3}) were calculated as the ratio of dried weight over fresh volume. Samples were oven-dried at 65°C for 48h, and fresh volume was determined by Archimedes' principle.

Results

Plant Structure

The length of stems along vertical wires was 12.7±1.8 m, exceeding (ANOVA, p=0.005) that of all other treatments (7.5±1.5, 2.4±0.6, 2.7±1.9, and 4.1±1.0 m for the 60°, 30°, 0° on wire

and 0° on ground, respectively). In all plants, the leaf area of individual leaves increased with path length in the 90° angle vines or when all data from the other growing angles were pooled (Figure 2A), as did the cross-sectional area of the petiole ($X_{petiole}$; Figure 2B) and the cross-sectional area of the stem xylem (X_{stem}; Figure 2C). However, within each of the 60°, 30°, and 0° treatments, stem area and leaf area of individual leaves did not increase with path length ($p>0.11$ for stems, and $p>0.32$ for leaves), likely reflecting the reduced stem length of these treatments. Specific leaf area did not change with path length (mean=247.5 $cm^2\ g^{-1}$; $p=0.82$). The length between leaves, *i.e.* the internode length $L_{internode}$, was conserved along a vine, but between vines grown at different angles, $L_{internode}$ was greater in vertical (29.7±1.7 cm) than horizontal stems (25.2±2.1 cm) (two-tailed t-test, $p=0.001$).

Tissue density varied from 0.21 g cm^{-3} in stem to 0.16 g cm^{-3} in petiole. Assuming a pure cell-wall density of 1.53 g cm^{-3} (Siau 1984), those values indicated that total cell wall represented 10.7% and 13.6% of the volume in petioles and stems, respectively. On average, parenchyma tissue represented between 61% (petiole) and 38% (stem) of the cross-sectional area. No differences in either tissue density or %parenchyma were detected among the three sampling heights ($p>0.4$ for stem, $p=0.18$ for petiole).

Separation between path length and height

Vines grown horizontally and at a 30° angle never reached more than 6 meters in length, thus limiting the comparison of vines characteristics as a function of path length versus height between specimens growing at different angles. Nevertheless, within this range, plant structural or functional characteristics were unaffected by the angle in which vines were trained to grow. Specifically, when controlling for the lowest common stem length of all treatments (i.e. less than 6 m), we found no angle-induced difference in non-transpiring ($p=0.37$) and transpiring ($p=0.52$) leaf water potentials, plant organ conductance ($p=0.39$ for leaves, $p=23$ for petioles, and $p=0.78$ for stems), and g_s ($p>0.19$). Thus, except for demonstrating the effect of height on predawn leaf water potential ($p=0.001$), and the effect of both height and distance from soil on g_s, all further analyses were performed on pooled data, evaluating how vines maintain g_s with path-length.

Gas Exchange

We found strong correlations among leaf-level gas exchange parameters (Figure S2). Decreasing g_s was directly related to changes in the ratio of intercellular CO_2 to ambient CO_2

(C_i/C_a), but only over low g_s values (up to ~0.25 mol m^{-2} s^{-1}), reflecting conditions of moderate-low PAR but high VPD (Figure S2A). Thus, once these low g_s values were exceeded, increases in g_s led to a nearly linear increase in A_{net} (Figure S2B). Estimates of V_{cmax} and the CO_2 compensation point were similar for leaves from the top and base of the 90° plants (t-test, p=0.34; Table 2).

Weather conditions for the periods of gas exchange and water potential measurements ranged from 0.5 to 3.5 kPa for VPD and from 200 to 1900 □mol m^2 s^{-1} for PAR (Figure S3A). Stomatal conductance decreased with increasing VPD and decreasing light intensity at a given VPD (Figure S3A; minimum r^2 was 0.59 for the lowest PAR interval, ranging from 0.70 – 0.71 for higher PAR intervals; maximum p=0.005). Each of the four PAR intervals was represented by stems of all four treatment angles. The sensitivity of g_s to ln(VPD) increased with g_{s-ref}, i.e. g_s at VPD=1kPa (Figure S3B). However, $g_{s\text{-}ref}$ increased significantly with PAR, showing little tendency to saturate at high irradiance (Figure S3C). Thus, although variation in g_s due to changes in soil moisture was eliminated through irrigation, the variation in g_s caused by varying atmospheric demand for water and light conditions must be considered before attributing the remaining variation in g_s to hydraulics.

To account for variation of g_s caused by VPD and PAR, we normalized all g_s values to their expected $g_{s\text{-}ref}$ (here referred to as $g_{s\text{-}ref}'$), and estimated the average maximum $g_{s\text{-}ref}'$ by relating these $g_{s\text{-}ref}'$ values to the actual PAR in which each original g_s value was measured (Figure 3A). Taking the residuals of this fit, and adding them to the fitted maximum $g_{s\text{-}ref}'$ (1.1 mol m^{-2} s^{-1} at a PAR of 2000 µmol m^{-2} s^{-1}; star in Figure 3A) we obtained $g_{s\text{-}ref}'m$. This final parameter is controlled by hydraulic architecture only, and was related to leaf height and to distance from the soil, showing only a weak relationship with both, with no difference between the linear slopes (p=0.87) relating $g_{s\text{-}ref}'m$ to either leaf height or distance to stem base (Figure 3B, C).

Water Potential

While no pattern emerged in daytime Ψ_{leaf} measurements with regard to either path length or height from the ground, for either the transpiring (p=0.52, 0°: p=0.94) or non-transpiring leaves (p=0.37, 0°: p=0.41), the predawn Ψ_{leaf} decreased significantly with height in the vertical treatment (p=0.001; Figure 4A), but not with length in the horizontal treatment (p=0.44), reflecting the expected effect of hydrostatic pressure. Transpiring Ψ_{leaf} was not significantly correlated to g_s (p=0.40) or E (p=0.71), and there was no clear difference in Ψ_{leaf}

of either transpiring leaves, or non-transpiring leaves (i.e. Ψ_{stem}) among the treatment angles (p=0.21; Figure 4B). Following the approach presented in Figure S3 and Figure 3, we accounted for the variation of Ψ_{leaf} caused by VPD and PAR. There was a decrease (p<0.02) in Ψ_{leaf} with increasing VPD and increasing light intensity at a given VPD. The resulting Ψ_{leaf} of transpiring leaves at $g_{s\text{-}ref}$ ($\Psi_{leaf\text{-}ref}$) decreased with increasing PAR (p=0.03), but $\Psi_{leaf\text{-}ref}$ of non-transpiring leaves was not significantly affected by irradiance (p=0.16; Figure 4C). We accounted for those variations by first calculating the residual of the decline in Ψ_{leaf} and Ψ_{stem} with VPD for a given PAR range, and added the value to the Ψ_{leaf} and Ψ_{stem} obtained from the same fit (Figure 4C), thus normalizing all Ψ_{leaf} and Ψ_{stem} values to their expected values at a VPD of 1 kPa. In the model, we used a constant $\Psi_{leaf\text{-}ref}$ (-0.97 MPa; transpiring leaf at maximum light, Figure 4C) and only accounted for the negative effect of the hydrostatic pressure on the water potential difference driving flow from soil to leaf.

Pressure-volume curves revealed that the turgor loss point of the vertically grown vines was more negative in leaves near the top of the tower than in lower leaves (ANOVA, p=0.047, Table 3). The osmotic potential at full turgor, the cell wall modulus of elasticity, and C_{leaf} were similar regardless of height (p>0.05). There was no difference in any of the parameters derived from the pressure-volume curves between the base and the tip of the horizontally grown vines (p=0.19), and between the base of the vertically and the horizontally grown vines (p=0.35).

Hydraulic Parameters

Neither K_{leaf}, averaging 24 mmol m^{-2} s^{-1} (Figure 5A), nor k_{s_stem}, averaging nearly 2000 mol m^{-1} s^{-1} (Figure 5C), varied significantly with stem height or path length. In contrast, $k_{s\_petiole}$ increased with increasing distance from the stem base (Figure 5B), yet there was no difference in the response between vines growing at 90° or at 0° angles (p=0.39). The theoretical k_s values calculated based on vessel anatomy were on average 3.8 times larger than the measured k_s values (paired t-test, p<0.001), but did not change with height (p=0.4).

Stems sampled from the top and base of each vine showed a similar pattern of reduction in conductivity as applied pressure increased. The applied pressure at which 50% of conductivity is lost (P_{50}) was not different between the tops and bases of vines on wires or on the ground (ANOVA, p=0.92). The average P_{50} for all stems was 2.1±0.1 MPa (Figure 6A). The daily loss in stem hydraulic conductivity reflecting the variations in stem pressures between pre-dawn and mid-day was similar (mean=7.5%) in the base and tops of vines on

wires, and on the ground at 0˚ (ANOVA, p=0.13). Stem hydraulic capacitance was 1.7 times greater than petiole capacitance (Figure 6B; z-test for slope coefficient, p=0.03).

Although significant, decreases of $g_{s\text{-}ref}'$m with both height and distance to stem base (from Figure 3B, C) were smaller compared to the theoretical decrease predicted by the DHF (when forced with a VPD of 1kPa and hydraulic parameters regressed from Figures 5 & 6), indicating an appreciable role of water storage (Figure 7A). The best fit of the model was with the assumption that the entire capacitance of kudzu tissues was linearly depleted over a 3-hour period. Doubling this time weakened the predictions in $g_{s\text{-}ref}'$m from the middle to the top of the vine. There was an increase in the capacitive effect of stored water with distance from the base of the vine, with capacitances representing 8% and 12% of the transpirational water flux at the base and at the top of the vine, respectively. The SHF model predicted reductions of g_s by >95% over the 15 m long stems, whereas the DHF model nearly matched the slight decreased in g_s (Figure 7A).

To maintain $g_{s\text{-}ref}'$m almost constant with height (calculated using a hypothetical plant with DHF and 3-hour depletion from stored water shown in Figure 7A) and yet support the higher leaf area measured here, water flow was predicted to double from the base to the top of the 90° vine, even when water storage was not taken into account (Figure 7B). Total plant resistance (the inverse of conductance) decreased more than 2-fold with path length (Figure 7C), and this trend was mostly driven by the decrease in lateral resistances (petiole and leaf). Those lateral resistances were three orders of magnitude larger than the axial resistance (stem resistance). Mirroring this increase in water delivery combined with the increase in individual leaf size with height, modeled carbon assimilation per leaf (using the relationship from Figure S2) was also estimated to more than double from the base to the top of the vine.

A series of analyses to test the sensitivity of $g_{s\text{-}ref}'m$ and water flows predictions to variation in the key parameters was performed (Table 4; Figure 8; Figure S4). These included specific conductivities, area, and length of each plant organ. Each of these parameters was varied individually, with the actual magnitude of variation applied in each case reflecting the observed variability in the parameter. The sensitivities of $g_{s\text{-}ref}'m$ and water flows were similar in form, though not always in magnitude (Figure 8; Figure S4). Water flows and $g_{s\text{-}ref}'m$ were most sensitive to changes in leaf size. Doubling leaf area at each node increased water flow only by a factor of 1.15 and halved $g_{s\text{-}ref}'m$, whereas dividing leaf area by 2 reduced water flow by a factor of 0.80, increasing $g_{s\text{-}ref}'m$ by a factor of 2. Lowering K_{leaf} by 50%, in turn, reduced both $g_{s\text{-}ref}'m$ and water flow by more than 20%. The effect of

modifying xylem conductivities was mixed, with large changes in $g_{s\text{-}ref}$*'m* at the base of the vine for $k_{s\_petiole}$, and more at the top for k_{s_stem}. As opposed to the base of the vine, $g_{s\text{-}ref}$*'m* at the top was not sensitive to changes in $k_{s\_petiole}$, petiole area or length.

Setting constant input parameters at each node, thus mimicking constant hydraulic and morphological attributes from base to top had some strong positive and negative effects on modelled water flow and $g_{s\text{-}ref}$*'m* values (Table 4; Figure 9). Setting individual leaf area in the DHF model as equal to that at the base of the vine increased $g_{s\text{-}ref}$*'m* by more than 100%, but had a negative effect on leaf water flow and carbon assimilation (data not shown in Table 4 but results for photosynthesis paralleled those for water flow, Figure 7B). On the other hand, both stem area and $k_{s\_petiole}$ were the strongest compensative parameters for the increase in leaf area with height and therefore had the largest influence on $g_{s\text{-}ref}$'m and water flow at the leaf but also at the whole-plant level (Figure 9). Forcing all parameters in the model with the values measured at the base would have doubled $g_{s\text{-}ref}$*'m* at the top of the vine (1.91 vs. 0.92 mol m^{-2} s^{-1}), however water flow and carbon assimilation per leaf and at the whole plant level would have been reduced by almost 50%.

Discussion

Contrary to our first hypothesis (Figure 1), we found no physiological differences among the vines growing in different orientation. Vines growing vertically did not show greater lateral relative to axial resistance than vines growing horizontally, and did not show a greater difference in water potential between leaves and soil, suggesting that vines grown at steeper angles did not have hydraulic traits that help compensate for height-driven declines in g_s compared to horizontally grown stems. This could simply reflect an inadequate challenge of the hypotheses, because horizontally-grown vines produced shorter stems (mostly < 7 meters). Alternatively, it may reflect the strict control kudzu imposes on water potential (Figure 4), not allowing tissues to develop very negative water potentials. This allowed us to combine the data regardless of stem orientation, and evaluate how vines maintain high stomatal conductance with path-length, representing vines climbing vertically on trees, stretching horizontally as mats over vegetation, and transitions among these end-member orientations (Figure 9).

Despite observations of steep declines in gas exchange rates with height in trees (Magnani et al., 2000; Schäfer et al., 2000; McDowell et al., 2002; Delzon et al., 2004; Renninger et al., 2009; Fang et al., 2013), studies in woody vines (Zhu & Cao, 2009;

Masrahi, 2014; Chen et al., 2015, Taneda & Tateno 2011) show that g_s remains high along the stem. Our results agree with these latter observations. Once the effects of temporal variation in irradiance and atmospheric vapor pressure deficit (VPD) during measurements were removed (Figure S3), we found only a slight (12%) reduction in the maximum reference stomatal conductance ($g_{s\text{-}ref}$'m) between the most basal and most distal leaves from the soil (Figure 3B). We found a similar decrease in $g_{s\text{-}ref}$'m with path length, regardless of height from the soil, indicating that physiological and structural changes with path length compensated for predicted height-related declines in maximum g_s. The path-length-related reduction in $g_{s\text{-}ref}$'m is averted by three primary compensating mechanisms related to changes in stem and petiole sapwood areas, petiole hydraulic conductivity ($k_{s\_petiole}$), and water supply from storage (Table 4).

Our measured g_s values under common field conditions (mean g_s = 0.45 mol m^{-2} s^{-1}; Figure 3) were similar to previous field observations of kudzu (Forseth & Teramura, 1987; Taneda & Tateno, 2011) and *Vitis* (Williams et al., 2012), but higher than others reported for other vine species (Lovisolo & Schubert, 1998; Johnson et al., 2013; van der Sande et al., 2013). Maintaining high g_s and transpiration rates along the stem is an effective way of cooling large leaves (Forseth & Teramura, 1987), supporting higher rates of net photosynthesis. Partial loss of leaf turgor was visible throughout the experiment by midday, suggesting that water delivery could not keep up with such high transpiration rates. Partial, diurnally reversible leaf wilting in kudzu may facilitate avoidance of high leaf temperatures because wilted leaves intercept less radiative energy.

Hydraulic Compensation

Our $g_{s\text{-}ref}$*'m* estimates represent g_s limited by plant hydraulics only and are thus the focus of the remaining discussion. We hypothesized that structural alterations would fully compensate for the limitation imposed on $g_{s\text{-}ref}$*'m* of kudzu as stem length increased (Figure 1), and that these alterations would be more pronounced in stems grown at steeper angles (and thus reaching greater heights from the soil). However, there was still a slight reduction in $g_{s\text{-}ref}$*'m* in vertical stems, driven in part by the declining water potential gradient (Figure 4C), as observed in trees (Ryan, Phillips & Bond, 2006; Domec et al., 2008) and other vines (Lovisolo & Schubert, 1998), and by the increase of individual leaf area with height (Figure 2A). In this experiment, daytime reference leaf water potential ($\Psi_{leaf\text{-}ref}$), representing Ψ_{leaf} at high light and a reference VPD = 1 kPa (Figure 4C), was roughly two-thirds of the minimum

Ψ_{leaf} reported in kudzu (Ponder & Al-Hamdani, 2011; Taneda & Tateno, 2011) and in other vines (Schultz & Matthews, 1988; Williams et al., 2012; Johnson et al., 2013; Tombesi et al., 2014), likely because the plants were well-watered and because actual Ψ_{leaf} can be lower at VPD > 1 kPa. While the gravitational effect on the vertically lengthening (but not horizontally oriented) water column was seen in the predawn pattern of Ψ_{leaf} (-0.01 MPa m^{-1}, Figure 4A), it was not apparent in daytime values of Ψ_{leaf}. There was an effect of stem growth angle on Ψ_{leaf} (Figure 4B) but, regardless of stem length or angle, transpiring leaves exposed to higher radiation had lower $\Psi_{leaf\text{-}ref}$ (Figure 4C), suggesting that in kudzu, $\Psi_{leaf\text{-}ref}$ is not controlled by leaf distance from the soil. Thus, for transpiring leaves, the gradient of water potential declined along the vine stem, not compensating for the increasing path length. Previous observations suggest that the largest kudzu leaves are located near the middle of the stem (Sasek & Strain, 1989), but we found that the size of individual leaves increased linearly from the base to the most distal nodes (Figure 2A). Nevertheless, despite a decreasing driving force for water flow and increasing individual leaf size, or node leaf area, up the vine, $g_{s\text{-}ref}$'m decreased only slightly with leaf height.

Even though no direct compensation was observed, i.e. no reduction in Ψ_{leaf} as height increased, kudzu could have potentially compensated in this way given that water potential at turgor loss point, Ψ_{TLP}, of the highest leaves was 24% more negative than Ψ_{TLP} of leaves near the ground (Table 3). Indeed, the average Ψ_{leaf} of transpiring leaves was only ~32% of the average Ψ_{TLP} (-1.2 MPa) observed in this study, and 20% of Ψ_{TLP} of other vines (Zhu & Cao, 2009; Johnson et al., 2013), suggesting that Ψ_{leaf} could decline further without risking leaf function.

Taneda & Tateno (2011) report a lamina resistance three times greater than ours (2.0 MPa s $mmol^{-1}$), stem resistance 3.6 times greater than ours (0.0025 MPa s $mmol^{-1}$) and petiole resistances 2.1 times lower than ours (2.2 MPa s $mmol^{-1}$) for kudzu. Moreover, the theoretical k_s values we calculated from stem vessel lumen diameters indicated that maximum k_{s_stem} could not be more than four times larger than the ones we measured. In addition, because those theoretical k_s values were more than twice greater than k_{s_stem}, it also indicated that in kudzu, conductivity is more wall-limited than lumen-limited (Hacke et al., 2006).

We combined regressions of tissue area and length with regressions of hydraulic conductivity to predict hydraulic resistance in each tissue at each node. While Schubert et al. (1999) report that conductance is more than double in stems grown vertically compared to stems angled downwards, we did not observe any treatment angle (or position) effect on stem hydraulic conductivity (k_{s_stem}; Figure 5C). However, in our study, $k_{s\_petiole}$ increased with

distance from the base (Figure 5B), in contrast to the lack of a pattern observed between $k_{s\_petiole}$ and position in previous studies of vines (Taneda & Tateno, 2011; Zufferey et al., 2011; Tombesi et al., 2014). Our measured conductivity values also explained why changing k_{s_stem} was predicted to have a stronger effect on $g_{s\text{-}ref}'m$ at the top than at the base of the vine, whereas the opposite was true for $k_{s\_petiole}$ (Figure 8). Lateral resistances dominated the overall plant water transport capacity in vines grown at all angles (Figure 7C), with the proportion of tissue-specific resistance to total plant resistance being 36% for leaves, 39% for petioles, and 3% for the stem, suggesting the remaining 22% of hydraulic resistance was located below ground. These greater lateral resistances to flow through the petiole and leaf likely allowed the upper leaves to be supplied with water equally as well as the lower leaves.

We hypothesized that structural changes with height would hydraulically compensate for path length limitations on g_s (Figure 1), hence providing distal leaves with sufficient water to support a nearly uniform transpiration rate (per unit leaf area) along the stem. Combining the hydraulic information summarized above into the SHF failed to explain the nearly complete hydraulic compensation observed in vertically-grown vines, as this model predicted reductions of $g_{s\text{-}ref}'m$ of >95% over the 15 m long stems (Figure 7A). However, the DHF model supported the hypothesis that structural and functional changes along the stem would produce only a slight decline in $g_{s\text{-}ref}'m$. Even though kudzu capacitance represented only 8% and 12% of the water flux at the base and at the top of the stem, respectively, these contributions of plant water storage must be considered for the model to agree with the observations (Figure 7A).

The relative contribution of stored water (mainly in stems) to total daily transpirational losses varies widely among species and ecosystems, ranging from 10% to 40% (see review by Scholtz et al., 2011). We assumed that the release of water storage to the transpirational stream was completed in either 3 or 6 hours. A 3-hour water discharge is consistent with the peak period of water use (between 08:00 and 11:00) from internal reservoirs in several fast-growing species (Bucci et al., 2003; Johnson et al., 2013), and in kudzu with the partial reversible leaf wilting that facilitates avoidance of high leaf temperatures (Lindgren et al., 2013). Water storage in plants can occur by three mechanisms: capillary storage, water release via embolism of xylem conduits, and shrinkage of parenchyma cells (Tyree & Yang, 1990). Capillary storage represents water that is available at high xylem water potential (0 to -0.25 MPa) and is inversely proportional to vessel size. Thus, release of capillary stored water may not represent a significant amount of water in large vessel-bearing vines or in tall individuals where xylem water potential is never close to zero. Furthermore, water release via embolism of vessels was

probably small, as the percent loss of conductivity (PLC) never exceeded 8% (Figure 6A), and in stems was likely represented by the points after the Ψ_{TLP} (Figure 6B). Thus, the capacitive discharge was apparently derived from parenchyma tissues that we found to represent a large portion of tissue volumes (>40%). Water released from elastic storage components may predominate in lianas and stem-succulent species, because xylem parenchyma occupies the majority of the total sapwood volume (Scholtz et al., 2011).

Possible Explanations for Uniform Water Delivery

Although plants have previously been shown to compensate for hydraulic limitations by increasing sapwood to leaf area ratio (Schäfer et al., 2000; Domec et al., 2012), increasing individual leaf area with distance to stem base (Figure 2A) led to a decreasing sapwood to leaf area ratio, suggesting that this is not a mechanism kudzu uses to compensate for hydraulic limitation (Figure 9). For this vine to attain the maximum transpiration rate along the entire stem while maintaining a constant leaf water potential set to the average value (Ψ_{leaf}=-0.97 MPa), it had to reduce its total resistance to the most distant leaves (Figure 7B). However, reducing the resistance in the stem will not have the same impact as reducing the resistance through the leaves or petioles (Figure S4).

The relative water delivery rate at the base versus the tip of a stem is determined by the ratio of the axial to lateral resistance, meaning that a large lateral resistance relative to the axial resistance is required to equalize flow to leaves distributed along long stems (Taneda & Tateno, 2011). This implies that increasing lateral resistance or decreasing stem resistance were necessary to recover the observed uniform flow rate. Kudzu internode resistance was 500-1000 times smaller than petiole resistance (Figure 7C), which indeed optimized water delivery along the main stem while at the same time inducing high Ψ_{stem} and, thus, preventing xylem embolism. This adjustment was accomplished through increasing stem areas with height rather than increasing k_{s_stem}. Yet, because k_{s_stem} was more limited by the resistance in the cell wall membrane than in the lumen, an increase in k_{s_stem} with height would have also decreased the resistance to embolism (Hacke et al., 2006). Thus, producing more conductive tissues rather than increasing the tissue permeability did not compromise resistance to embolism. However, increasing stem biomass per unit length, associated with increasing cross-sectional area, requires greater carbon assimilation at heights, thus constraining further increases in leaf area.

Finally, without any changes in resistances with height, more negative Ψ_{leaf} could not have compensated for the increase of leaf area at higher positions. To reach maximum flow using constant resistances throughout the stems, leaves at 15 m height would have to drop their Ψ_{leaf} to <-1.9 MPa, nearly 0.7 MPa below Ψ_{TLP} at any position (Table 3). Alternatively, kudzu could use positive root pressure to increase $\Delta\Psi$, but observations of root pressure in vines are well below 0.7 MPa (Clearwater et al., 2007), far from the 1.9 MPa required.

Conclusions

Fast-growing vines such as kudzu must supply all leaves with sufficient water to maintain high photosynthetic rates and fast growth rates far from the roots. We found no physiological difference in vine stems growing at different orientations but were able to identify the main structural (increasing petiole and stem sapwood area) and functional (decreasing petiole hydraulic resistance) mechanisms supporting a nearly uniform supply of water per unit leaf area along the stem. In addition, large lateral relative to axial hydraulic resistance helped even water flow distribution with height. However, the decreases of stomatal conductance with distance to the stem base were smaller compared to the theoretical values predicted by the distributed hydraulic formulation model, indicating an appreciable role of water storage in supplying water for transpiration to leaves near the top of the vine. Combining the only slightly decreasing stomatal conductance along the stem with increasing leaf size and path-length-invariable maximum carboxylation rate provides for increasing leaf-scale photosynthesis with distance from the vine base and a local source of carbohydrates to support the high growth rates observed at the top of kudzu stems.

Funding information. This work was supported by a grant from the National Science Foundation (NSF-IOS-1754893 & NSF-DEB-1557176), and from the US–Israeli Bi-national Science Foundation (#2010320)

References

Ambrose AR, Sillett SC, Koch GW, Van Pelt R, Antoine ME, Dawson TE. (2010). Effects of height on treetop transpiration and stomatal conductance in coast redwood (*Sequoia sempervirens*). *Tree Physiology, 30*, 1260-1272.

Andrade JL, Meinzer FC, Goldstein G, Holbrook NM, Cavelier J, Jackson P, Silvera K. (1998). Regulation of Water Flux through Trunks, Branches, and Leaves in Trees of a Lowland Tropical Forest. *Oecologia, 115*, 463-471.

Bohrer G, Mourad H, Laursen TA, Drewry D, Avissar R, Poggi D, Oren R, Katul GG. (2005). Finite element tree crown hydrodynamics model (FETCH) using porous media flow within branching elements: A new representation of tree hydrodynamics. *Water Resources Research, 41*, W11404-17.

Bucci SJ, Scholz FG, Goldstein G, Meinzer FC, Sternberg LD. (2003). Dynamic changes in hydraulic conductivity in petioles of two savanna tree species: factors and mechanisms contributing to the refiling of embolized vessels. *Plant, Cell & Environment, 26*, 1633–1645.

Calkin HW, A.C. Gibson, Nobel PS. (1986). Biophysical model of xylem conductance in tracheids of the fern *Pteris vittata*. *Journal of Experimental Botany, 37*, 1054–1064.

Carter GA, Teramura AH. (1988). Vine photosynthesis and relationships to climbing mechanics in a forest understory. *American Journal of Botany, 75*, 1011-1018.

Chen YJ, Cao, KF, Schnitzer SA, Fan ZX, Zhang JL, Bongers F. (2015). Water-use advantage for lianas over trees in tropical seasonal forests. *New Phytologist, 205*, 128-136.

Clearwater MJ, Blattmann P, Luo Z, Lowe RG. (2007). Control of scion vigour by kiwifruit rootstocks is correlated with spring root pressure phenology. *Journal of Experimental Botany, 58*, 1741-1751.

Clearwater MJ, Lowe RG, Hofstee BJ, Barclay C, Mandemaker AJ, Blattmann P. (2004). Hydraulic conductance and rootstock effects in grafted vines of kiwifruit. *Journal of Experimental Botany, 55*, 1371-1382.

Delzon S, Sartore M, Burlett R, Dewar R, Loustau D. (2004). Hydraulic responses to height growth in maritime pine trees, *Plant, Cell & Environment, 27*, 1077–1087.

Domec JC, Lachenbruch B, Meinzer FC, Woodruff DR, Warren JM, McCulloh KA. (2008). Maximum height in a conifer is associated with conflicting requirements for xylem design. *Proceedings of the National Academy of Sciences of the United States of America, 105*, 12069-12074.

Domec JC, Pruyn M, Lachenbruch B and Spicer R. (2012). Effects of age-related increases in sapwood area, leaf area, and xylem conductivity on height-related hydraulic costs in two contrasting coniferous species. *Annals of Forest Science, 69*, 17-27.

Edwards WRN, Jarvis PG, Landsberg JJ, Talbot H. (1986). A dynamic model for studying flow of water in single trees. *Tree Physiology 1*, 309-324.

Ennajeh M, Nouiri M, Khemira H, Cochard H. (2011). Improvement to the air-injection technique to estimate xylem vulnerability to cavitation. *Trees* 25, 705-710.

Ewers FW, Zimmermann MH. (1984). The hydraulic architecture of balsam fir (*Abies balsamaea*). *Physiologia Plantarum, 60*, 453-458.

Ewers FW, Fisher JB. (1989). Techniques for measuring vessel lengths and diameters in stems of woody plants. *American Journal of Botany, 76*, 645-56.

Ewers BE, Oren R, Johnsen KH, Landsberg JJ. (2001). Estimating maximum mean canopy stomatal conductance for use in models. *Canadian Journal of Forest Resources, 31*, 198–207.

Ewers BE, Oren R, Bohrer G, Lai CT. (2007). Effects of Hydraulic Architecture and Spatial Variation in Light on Mean Stomatal Conductance of Tree Branches and Crowns. *Plant, Cell and Environment, 30*, 483-496.

Fang XW, Turner NC, Xu DH, Jin Y, He J, Li FM. (2013). Limits to the height growth of *Caragana korshinskii* resprouts. *Tree Physiology, 33*, 275-284.
Farquhar GD, von Caemmerer S, Berry JA. (1980). A biochemical model of photosynthetic CO2 assimilation in leaves of C 3 species. *Planta, 149*, 78-90.
Filartiga AL, Vieira RC, Mantovani A, Rennenberg H. (2014). Size-correlated morpho-physiology of the aroid vine Rhodospatha oblongata along a vertical gradient in a Brazilian rain forest. *Plant Biology, 16*, 155-165.
Forseth IN, Teramura AH. (1987). Field photosynthesis, microclimate and water relations of an exotic temperate liana, *pueraria lobata*, kudzu. *Oecologia, 71*, 262-267.
Gartner BL. (1991). Stem hydraulic properties of vines vs. shrubs of western poison oak, *toxicodendron diversilobum*. *Oecologia, 87*, 180-189.
Hacke UG, Sperry JS, Wheeler JK, Castro L. (2006). Scaling of angiosperm xylem structure with safety and efficiency. *Tree Physiology, 26*, 619–701
Huang CW, Chu CR, Hsieh CI, Palmroth S, Katul, G.G. (2015). Wind-induced leaf transpiration. *Advances in Water Resources, 86*, 240–255.
Huang CW, Domec JC, Ward EJ, Duman T Manoli, G, Parolari AJ, Katul GG. (2017). The effect of plant water storage on water fluxes within the coupled soil-plant system. *New Phytologist, 213*, 1093–1106.
ISSG. 2013. 100 of the world's worst invasive alien species. *Pueraria montana* val. *lobata. http://www.issg.org/database/species/search.asp?st=100ss&fr=1&sts*
Johnson DM, Domec JC, Woodruff DR, McCulloh KA, Meinzer FC. (2013). Contrasting hydraulic strategies in two tropical lianas and their host trees. *American Journal of Botany, 100*, 374-383.
Johnson, D. M., Wortemann, R., McCulloh, K. A., Jordan-Meille, L., Ward, E., Warren, J. M., … Domec, J.-C. (2016). A test of the hydraulic vulnerability segmentation hypothesis in angiosperm and conifer tree species. *Tree Physiology, 36*, 983–993.
Jones HG. (1992). Plant and microclimate: a quantitative approach to environmental plant physiology. Cambridge (England), Cambridge University Press.
Lindgren CJ, Castro KL, Coiner HA, Nurse RE, Darbyshire SJ. (2013). The biology of invasive alien plants in Canada. *Pueraria montana* var. *lobata* (Willd.) Sanjappa & Predeep. *Canadian Journal of Plant Science, 93*, 71–95.
Lovisolo C, Schubert A. (1998). Effects of water stress on vessel size and xylem hydraulic conductivity in Vitis. *Journal of Experimental Botany, 49*, 693-700.
Magnani F, Mencuccini M, Grace J. (2000). Age-related decline in stand productivity: the role of structural acclimation under hydraulic constraints. *Plant, Cell and Environment, 23*, 251-263.
Masrahi YS. (2014). Ecological significance of wood anatomy in two lianas from arid southwestern Saudi Arabia. *Saudi Journal of Biological Sciences, 21*, 334–341.
McDowell NG, Phillips N, Lunch C, Bond BJ, Ryan MG. (2002). An investigation of hydraulic limitation and compensation in large, old Douglas-fir trees. *Tree Physiology, 22*, 763-774.
Meinzer FC. (2002). Co-ordination of vapour and liquid phase water transport properties in plants. *Plant, Cell & Environment* 25, 265–274.
Meinzer FC, Woodruff DR, Domec JC, Goldstein G, Campanello PI, Genoveva Gatti M, Villalobos-Vega R. (2008). Coordination of leaf and stem water transport properties in tropical forest trees. *Oecologia, 156*, 31– 41.
Melcher P J, Holbrook NM, Burns MJ, Zwieniecki MA, Cobb AR, Brodribb TJ, Choat B. (2012) Measurements of stem xylem hydraulic conductivity in the laboratory and field. *Methods in Ecology and Evolution, 3*, 685–694.

Mencuccini MJ, Grace J, Fioravanti M. (1997). Biomechanical and hydraulic determinants of tree structure in Scots pine: Anatomical characteristics. *Tree Physiology, 17*, 105-113.
Niinemets U. (2010). A review of light interception in plant stands from leaf to canopy in different plant functional types and in species with varying shade tolerance. *Ecological Research, 15*, 693-714.
Nolan RH, Mitchell PJ, Bradstock RA, Lane PN. (2014). Structural adjustments in resprouting trees drive differences in post-fire transpiration. *Tree physiology, 34*, 123-136.
Novick K, Oren R, Stoy P, Juang JY, Siqueira M, Katul G. (2009). The relationship between reference canopy conductance and simplified hydraulic architecture. *Advances in Water Resources, 32*, 809-819.
Oren R, Sperry JS, Katul GG, Pataki DE, Ewers BE, Phillips N, Schäfer KVR. (1999). Survey and synthesis of intra- and interspecific variation in stomatal sensitivity to vapour pressure deficit. *Plant, Cell & Environment, 22*, 1515–1526.
Pennisi E. 2005. Tree growth: the sky is not the limit. *Science, 310*, 1896-1897.
Phillips N, Bond BJ, McDowell NG, Ryan MG, Schauer A. (2003). Leaf Area Compounds Height-Related Hydraulic Costs of Water Transport in Oregon White Oak Trees. *Functional Ecology, 17*, 832-840.
Ponder DM, Al-Hamdani SH. (2011). Selected physiological responses of kudzu to different levels of induced water stress. *Journal of the Alabama Academy of Science,* 82, 44-46.
Pratt RB, Jacobsen AL (2017). Conflicting demands on angiosperm xylem: Tradeoffs among storage, transport, and biomechanics. *Plant Cell & Environment*, 40, 897–913.
Renninger HJ, Phillips N, Hodel DR. (2009). Comparative Hydraulic and anatomic properties in palm trees (*Washingtonia robusta*) of Varying heights: implications for hydraulic limitation to increased height growth. *Trees, 23*, 911-921.
Restom TG, Nepstad DC. (2001). Contribution of vines to the evapotranspiration of a secondary forest in eastern Amazonia. *Plant and Soil, 236*, 155-163.
Richter H. (1997) Water relations of plants in the field: some comments on the measurement of selected parameters. *Journal of Experimental Botany, 48*, 1-7.
Rosell JA, Olson ME. (2014). Do lianas really have wide vessels? Vessel diameter-stem length scaling in non-self-supporting plants. *Perspectives in Plant Ecology, Evolution and Systematics, 16*, 288-295.
Running SW. (1980). Field estimates of rot and xylem resistances in *Pinus contorta* using root excision. *Journal of Experimental Botany, 31*, 555-569.
Ryan MG, Yoder BJ. (1997). Hydraulic limits to tree height and tree growth. *BioScience, 47*, 235-242.
Ryan MG, Bond BJ, Law BE, Hubbard RM, Woodruff D, Cienciala E, Kucera J. (2000). Transpiration and whole-tree conductance in ponderosa pine trees of different heights. *Oecologia, 124*, 553-560.
Ryan MG, Phillips N, Bond BJ. (2006). Hydraulic limitation hypothesis revisited. *Plant, Cell & Environment, 29*, 367-381.
Sasek TW, Strain BR. (1989). Effects of Carbon Dioxide Enrichment on the Expansion and Size of Kudzu (*Pueraria lobata*) Leaves. *Weed Science, 37*, 23-28.
Schäfer KVR, Oren R, Tenhunen JD. (2000). The effect of tree height on crown-level stomatal conductance. *Plant, Cell & Environment, 23*, 365-377.
Scholz FG, Phillips NG, Bucci SJ, Meinzer FC, Goldstein G. (2011). *Hydraulic capacitance: biophysics and functional significance of internal water sources in relation to tree size*. In: Size- and Age-Related Changes in Tree Structure and Function (eds F.C. Meinzer, B. Lachenbruch & T.E. Dawson). Springer, Dordrecht.

Schubert A, Lovisolo A, Peterlunger E. (1999). Shoot orientation affects vessel size, shoot hydraulic conductivity and shoot growth rate in *Vitis vinifera* L. *Plant, Cell & Environment, 22*, 197–204.
Schultz H, Matthews M. (1988). Resistance to water transport in shoots of *Vitis vinifera* L. *Plant Physiology, 88*, 718-724.
Siau JF. (1984). *Transport processes in wood*. Springer Verlag, Berlin, Heidelberg, New York, Tokyo.
Sperry J, Saliendra NZ. (1994). Intra- and inter-plant variation in xylem cavitation in *Betula occidentalis*. *Plant Cell and Environment, 17*, 1233-1241.
Sperry JS, Hacke UG, Oren R, Comstock JP. (2002). Water deficits and hydraulic limits to leaf water supply. *Plant, Cell and Environment, 25*, 251-263.
Sperry JS, Hacke UG, Wheeler KJ. *(*2005). Comparative analysis of end wall resistivity in xylem conduits. *Plant, Cell & Environment, 38*, 456–465.
Stokes VJ, Morecroft MD, Morison J. (2006). Boundary layer conductance for contrasting leaf shapes in a deciduous broadleaved forest canopy. *Agricultural and Forest Meteorology, 139*, 40-54.
Taneda H, Tateno M, (2007). Effects of transverse movement of water in xylem on patterns of water transport within current-year shoots of kudzu vine, *Pueraria lobata*. *Functional Ecology, 21*, 226-234.
Taneda H, Tateno M. (2011). Leaf-lamina conductance contributes to an equal distribution of water delivery in current-year shoots of kudzu-vine shoot, *Pueraria lobata*. *Tree Physiology, 31*, 782-794.
Tombesi S, Nardini A, Farinelli D, Palliotti A. (2014). Relationships between stomatal behavior, xylem vulnerability to cavitation and leaf water relations in two cultivars of *Vitis vinifera*. *Physiologia Plantarum, 152*, 453–464.
Tor-ngern P., Oren R, Ward E, Palmroth S, McCarthy H, Domec JC. (2015). Increases in atmospheric CO2 have little influence on transpiration of a temperate forest canopy. *New Phytologist, 205*, 215-218.
Tsuda M, Tyree MT. (1997). Whole-plant hydraulic resistance and vulnerability segmentation in *Acer saccharum*. *Tree Physiology*, 17, 351-357.
Tyree MT, Hammel HT. (1972). The measurement of the turgor pressure and the water relations of plants by the pressure-bomb technique. *Journal of Experimental Botany,* 23, 267-282.
Tyree MT, Yang S. (1990). Water storage capacity of *Thuja*, *Tsuga* and *Acer* stems measured by dehydration isotherms: the contribution of capillary water and cavitation. *Planta,* 182, 420-426.
Van den Honert TH. (1948). Water transport as a catenary process. *Faraday Society Discussion,* 3, 146–153.
van der Sande MT, Poorter L, Schnitzer SA, Markesteijn L. (2013). Are lianas more drought-tolerant than trees? A test for the role of hydraulic architecture and other stem and leaf traits. *Oecologia,* 172, 961-972.
Venturas MD, Sperry JS, Hacke UG. (2017). Plant xylem hydraulics: What we understand, current research, and future challenges. Journal of Integrative *Plant Biology*, 59, 356–389.
Whitehead D, Edwards WRN, Jarvis PG. (1984). Conducting sapwood area, foliage area, and permeability in mature trees of *Picea sitchensis* and *Pinus contorta*. *Canadian Journal of Forest Research,* 14, 940-947.
Whitehead D, Hinckley T. (1991). Models of water flux through forest stands: critical leaf and stand parameters. *Tree Physiology*, 9, 35-57.
Whitehead D. (1998). Regulation of stomatal conductance and transpiration in forest canopies. *Tree Physiology,* 18, 633–644.

Williams LE, Baeza P, Vaughn P. (2012). Midday measurements of leaf water potential and stomatal conductance are highly correlated with daily water use of thompson seedless grapevines. *Irrigation Science,* 30, 201-212.

Williams M, Rastetter EB, Fernandes DN, Goulden ML, Wofsy SC, Shaver GR, Melillo JM, Munger JW, Fan S-M, Nadelhoffer KJ. (1996). Modelling the soil-plant-atmosphere continuum in a *quercus-acer* stand at Harvard forest: The regulation of stomatal conductance by light, nitrogen and soil/plant hydraulic properties. *Plant, Cell & Environment,* 19, 911-927.

Woodruff DR, Bond BJ, Meinzer FC. (2004). Does turgor limit growth in tall trees? *Plant, Cell & Environment,* 27, 229–236.

Zhu S, Cao K. (2009. Hydraulic properties and photosynthetic rates in co-occurring lianas and trees in a seasonal tropical rainforest in southwestern china. *Plant Ecology,* 204, 295-304.

Zimmermann MH. (1983). *Xylem Structure and the Ascent of Sap*. Berlin (Germany): Springer-Verlag.

Zufferey V, Cochard H, Ameglio T, Spring JL, Viret O. (2011). Diurnal cycles of embolism formation and repair in petioles of grapevine (*Vitis vinifera* cv. Chasselas). *Journal of Experimental Botany,* 62, 3885-3894.

Table 1. Symbols, Units and Description of Variables

Symbol	Description	Units
A_{net}	Net rate of carbon assimilation	μmol m^{-2} s^{-1}
C_a	Atmospheric CO_2 concentration	ppm
C_i	Leaf internal CO_2 concentration	ppm
E_k	Driving force for flow in Ohm's Law analogy	MPa
g_s	Stomatal conductance to water vapor	mol m^{-2} s^{-1}
$g_{s\text{-}ref}$	Reference stomatal conductance, at VPD=1 kPa	mol m^{-2} s^{-1}
$g_{s\text{-}ref}$'m	Maximum reference stomatal conductance, at VPD=1 kPa and 2000	mol m^{-2} s^{-1}
g_b	Boundary layer conductance	mol m^{-2} s^{-1}
h	Height above the ground	m
$I_{Axial,k}$	Water flow rate through axial pathway between kth node and	mmol s^{-1}
$I_{Lateral,k}$	Water flow rate through lateral pathway at kth node	mmol s^{-1}
K_{leaf}	Leaf hydraulic conductance	mol m^{-2} s^{-1} MPa^{-1}
$k_{s\_petiole}$	Petiole xylem specific hydraulic conductivity	mol m^{-1} s^{-1} MPa^{-1}
k_{s_stem}	Stem xylem specific hydraulic conductivity	mol m^{-1} s^{-1} MPa^{-1}
$L_{internode}$	Internode length, distance between adjacent leaves	m
L_{leaf}	Mean leaf length	m
L_{path}	Path length	m
$L_{petiole}$	Petiole length	m
N	Total number of nodes	integer
P_{50}	Xylem pressure to induce 50% loss of k_{s_stem}	MPa
PAR	Photosynthetically active radiation	μmol m^{-2} s^{-1}
$R_{Axial,k}$	Resistance through axial pathway at node k	MPa s $mmol^{-1}$
$R_{Lateral,k}$	Resistance through lateral pathway at kth node	MPa s $mmol^{-1}$
R_{leaf}	Leaf hydraulic resistance	MPa s $mmol^{-1}$
$R_{petiole}$	Petiole specific resistance	MPa s $mmol^{-1}$
R_{stem}	Internode (stem) resistance	MPa s $mmol^{-1}$
T_{air}	Air Temperature	°C
$S_{Axial,k}$	Storage flow rate in stem between kth node and (k+1)th node	mmol H_2O s^{-1}
$S_{Lateral,k}$	Storage flow rate in petiole and leaf at kth node	mmol H_2O s^{-1}
u	Wind velocity	m s^{-1}
V_{cmax}	Maximum Rubisco carboxylation rate	μmol m^{-2} s^{-1}
VPD	Vapor Pressure Deficit	kPa
X_{stem}	Stem cross sectional xylem area	m^2
$X_{petiole}$	Petiole cross sectional area	m^2
$\Delta\Psi$	Water potential difference of the soil-to-leaf pathway	MPa
Ψ_{leaf}, Ψ_{soil}	Leaf and soil water potentials	MPa

Table 2. Results from A_{net}/C_i analysis (mean±SE, n=8) measured at 30ºC indicate no statistical difference between the upper leaves and the lower leaves on the vertical *P. lobata* vines.

Average Leaf Height (m)	CO_2 Compensation point (ppm)	V_{cmax} (µmol CO_2 m^{-2} s^{-1})
13.1±0.4	69.7±3.6	63.8±9.4
1.2±0.1	63.7±4.7	75.1±12.1

Table 3. Leaf pressure-volume curve analysis (mean±SE) showing the water potential at the turgor loss point (Ψ_{TLP}), the osmotic potential at full turgor (Ψ_{FT}), the cell wall modulus of elasticity (ε_{max}), and the leaf capacitance (C_{leaf}). No significant differences exist between the top, base, or ground vines for any parameters ($p>0.1$) except for Ψ_{TLP}. Different superscripted letters indicate significant differences between leaf locations ($p<0.05$).

Leaf Location	n	Ψ_{TLP} (MPa)	Ψ_{FT} (MPa)	ε_{max} (MPa)	C_{leaf} (g m^{-2} MPa^{-1})
Top (14m)	6	-1.28±0.07^{a}	-1.05±0.10	30.1±7.7	22.9±2.4
Base (1.4 m)	6	-1.21±0.09^{ab}	-1.01±0.11	23.3±3.1	27.7±5.1
Ground (0.3m)	8	-1.03±0.06^{b}	-0.86±0.05	18.7±2.4	19.8±2.3

Table 4. Effect of using constant input parameters (values at the base of the vine used in the Distributed Hydraulic Formulation (DHF) model were taken as references) at each node on the computed reference stomatal conductance ($g_{s\text{-}ref}'m$) and water flow at the top of the canopy. The input new values were changed one at the time, except for the "All parameters" row. The capacitance parameter represents the sum of leaf, petiole and stem capacitances (C_{leaf}, $C_{petiole}$, and C_{stem}) and is given on a leaf area basis. The mean percentage deviation from the standard runs at the top are also shown. For reference, $g_{s\text{-}ref}'m$ at the top of the vine in the original DHF model was 0.92 mol m^{-2} s^{-1}.

Parameter	Input values			$g_{s\text{-}ref}'m$ at top		Flow at top	
	Original (top DHF)	New (base DHF)	% change	New value	% change	New value	% change
Leaf Water potential (MPa)	-0.83	-0.97	17	1.15	25	0.19	21
Leaf area (cm^2)	385	153	-60	1.96	113	0.09	-39
Petiole area (mm^2)	5.4	2.6	-53	0.76	-17	0.13	-15
Stem sapwood area (mm^2)	40.3	12.5	-69	0.46	-50	0.10	-35
K_{leaf} (mmol m^{-2} $s^{-1}$$MPa^{-1}$)	23	23	0	0.92	0	0.16	0
$k_{s\_petiole}$ (kg m^{-1} s^{-1} MPa^{-1})	0.72	1.89	-74	0.61	-34	0.11	-30
k_{s_stem} (kg m^{-1} s^{-1} MPa^{-1})	31.2	31.2	0	0.92	0	0.16	0
Capacitance (g m^{-2} MPa^{-1})	157	130	-17	0.87	-5	0.16	0
g_{bl} (mol m^{-2} s^{-1})	2.2	2.8	27	0.84	-9	0.16	0
Mean			-28		3		-11
All parameters				1.91	108	0.07	-53

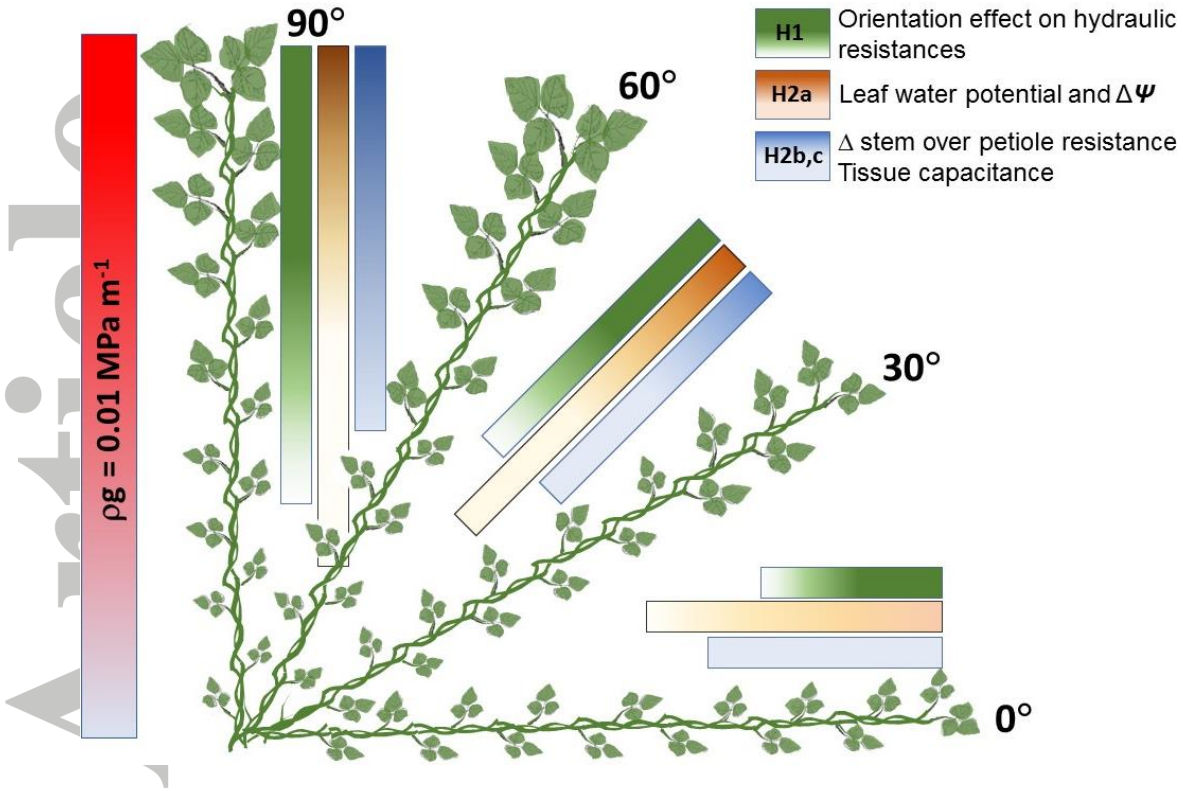

Figure 1. Conceptual figure showing how hydraulic traits related to the stated hypotheses (H) may change with height within Kudzu. Note that individual node leaf area is expected to increase with height. Length of bars and color gradients depict the effect of vine orientation on absolute trait values and the change of these values within a given orientation, respectively. Gravitational potential increases vertically 0.01 MPa for every meter, which contributes to reductions in the water potential gradient ($\Delta\Psi$) with height.

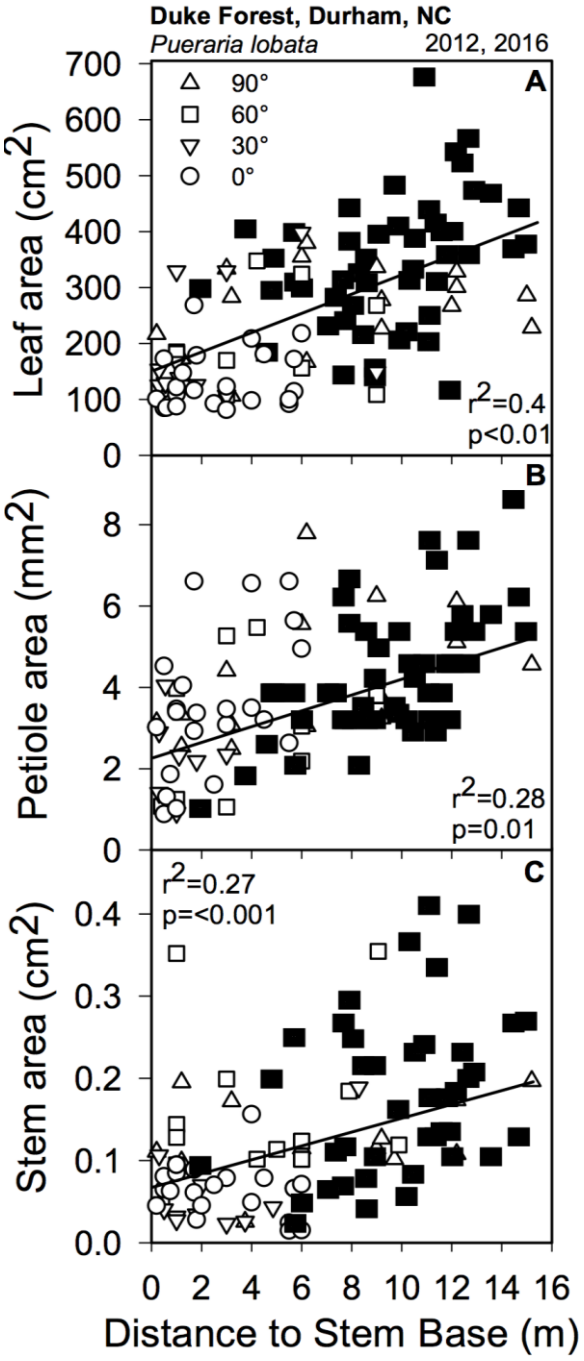

Figure 2. **A**. Individual leaf area, **B**. petiole xylem area ($X_{petiole}$), and **C**. stem cross-sectional xylem area (X_{stem}) increase with distance from the base of the kudzu stem in the 90° angle vines or when all data from the other growing angles were pooled. The responses of leaf area and $X_{petiole}$ is similar in all treatment angles, the response of X_{stem} is significant in the 60° and 90° treatments, but there is no trend in the 0° and 30° treatments. Filled symbols correspond to supplemental data collected in 2016 on vines growing in natural conditions.

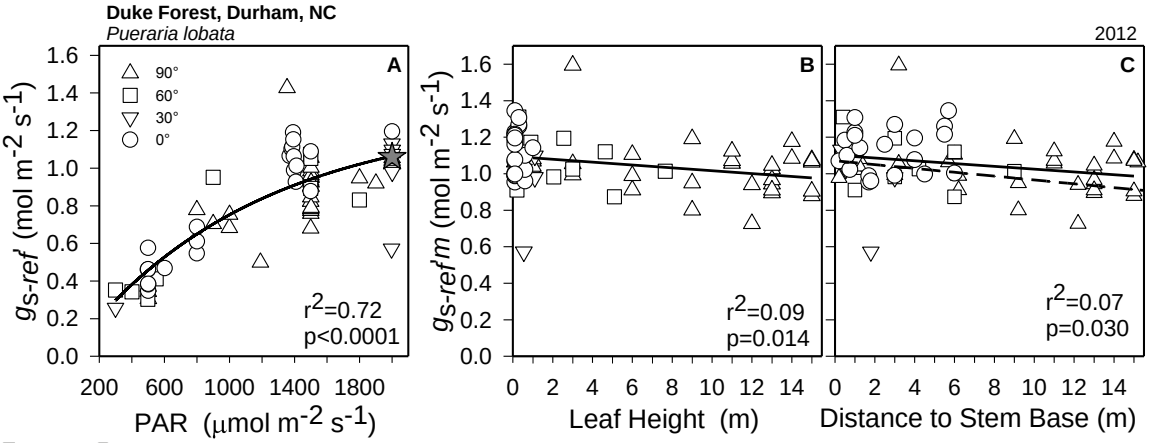

Figure 3. **A**. Increase in kudzu reference stomatal conductance ($g_{s\text{-}ref}$) with photosynthetically active radiation (PAR) (Star indicates the average conductance at maximum observed PAR). Maximum $g_{s\text{-}ref}$ ($g_{s\text{-}ref}$'m, estimated at PAR=2000 μmol m^{-2} s^{-1}) decreases slightly with **B**. leaf height, and **C**. hydraulic path. There was no difference between the linear slopes (p=0.87) relating $g_{s\text{-}ref}'m$ to either leaf height in **B**. or to distance to stem base in **C**. Dashed line in **C.** indicates a decrease proportional to the gravitational effect on the force driving water flow, beginning at 1 MPa at the base.

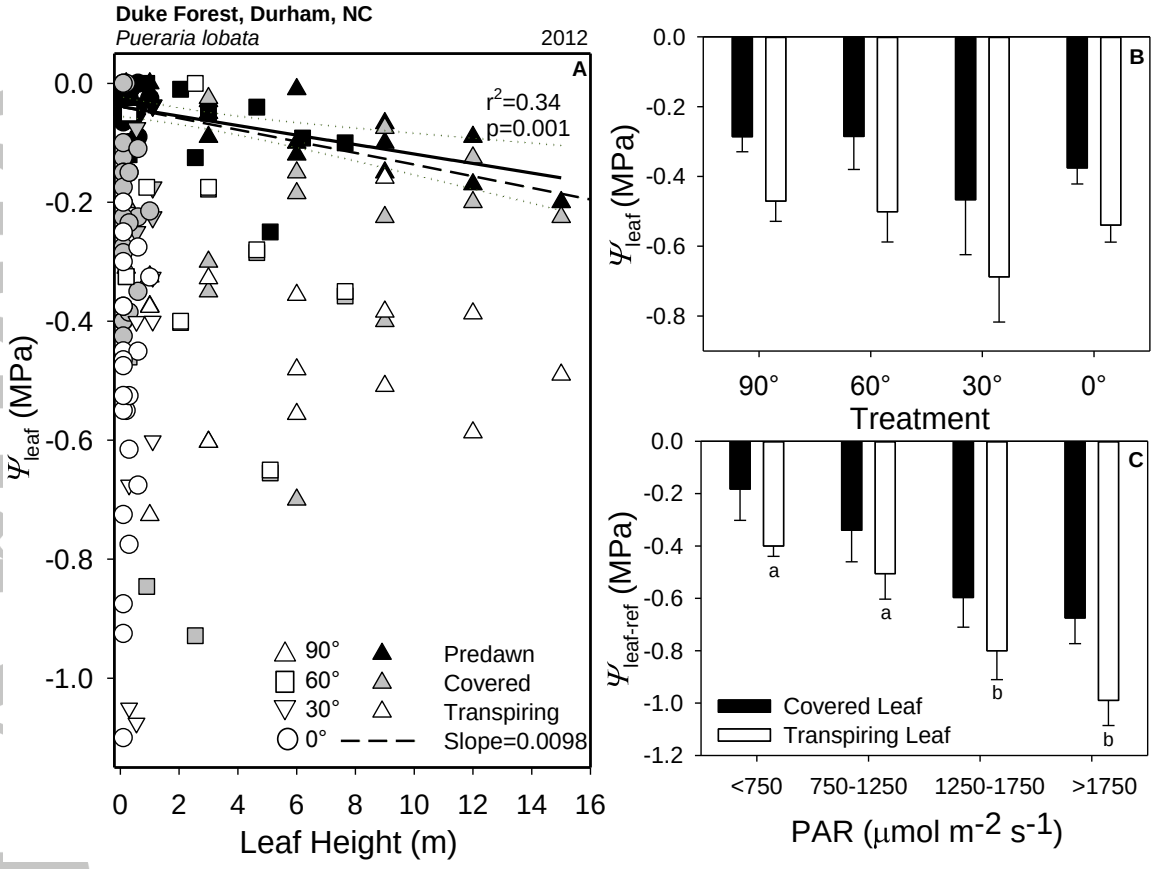

Figure 4. A. No pattern in Kudzu leaf water potential (Ψ_{leaf}) emerged with increasing path length or height from the ground, while predawn Ψ_{leaf} decreased significantly with height. The predicted slope for the pre-dawn data falls within the 95% confidence interval of linear regression (slope=0.009 MPa m^{-1}). No significant height effect was detected on the water potential of non-transpiring covered leaves (corresponding to stem water potential, Ψ_{stem}) and transpiring leaves during morning hours. **B**. Leaf water potential of neither transpiring nor non-transpiring leaves differed among the stem angle treatments. **C**. Leaf water potential of transpiring leaves at $g_{s\text{-}ref}$'m ($\Psi_{leaf\text{-}ref}$) decreased with increasing photosynthetically active radiation (PAR), but that of non-transpiring covered leaves was not significantly affected. Error bars are SE.

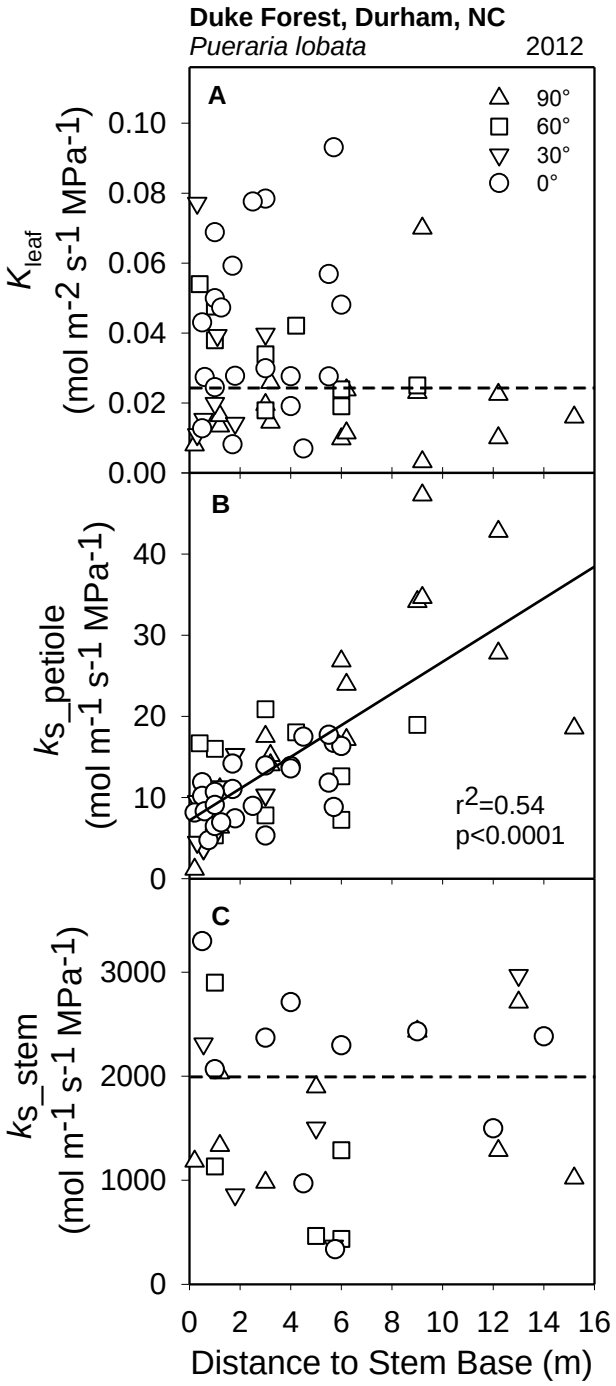

Figure 5. **A**. Leaf conductance (K_{leaf}) does not vary with distance to kudzu stem base. **B**. Petiole hydraulic specific conductivity ($k_{s\_petiole}$) increases with length across all treatment angles. **C** Stem specific conductivity (k_{s_stem}) does not vary with distance to stem base.

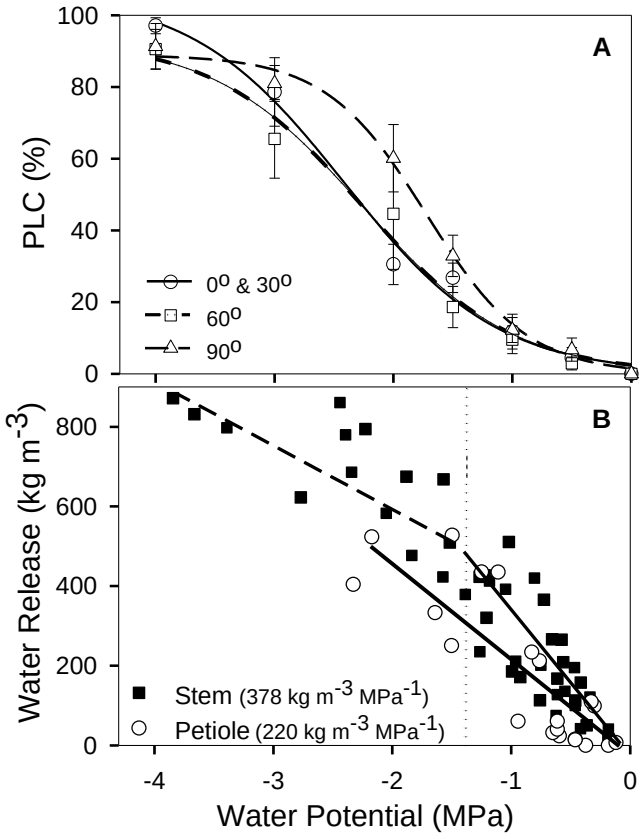

Figure 6. A. Kudzu stems from the top and base of each vine showed a similar pattern of percent loss of conductivity (PLC) for samples growing at 0°, 30°, 60°, 90° as applied pressure increased. **B**. Volumetric moisture release curves for stems (squares) and petioles (circles). Mean capacitance values (C_{stem} and $C_{petiole}$) were calculated as the slope of the relationship between water potential and water release. In stem, high C_{stem} was found before the turgor loss point (full line). Post turgor loss C_{stem} (slope of dashed line) decreased significantly (p=0.02). No differences were found in $C_{petiole}$ before and after the turgor loss point (full line through petiole data). The initial linear regression between xylem water potential and water release for the stem samples (r^2=0.69) was significantly different to the linear regression (r^2=0.72) for the petioles. The grey, vertical shaded areas and the dotted line are the average leaf water potentials at midday and the turgor loss point, respectively.

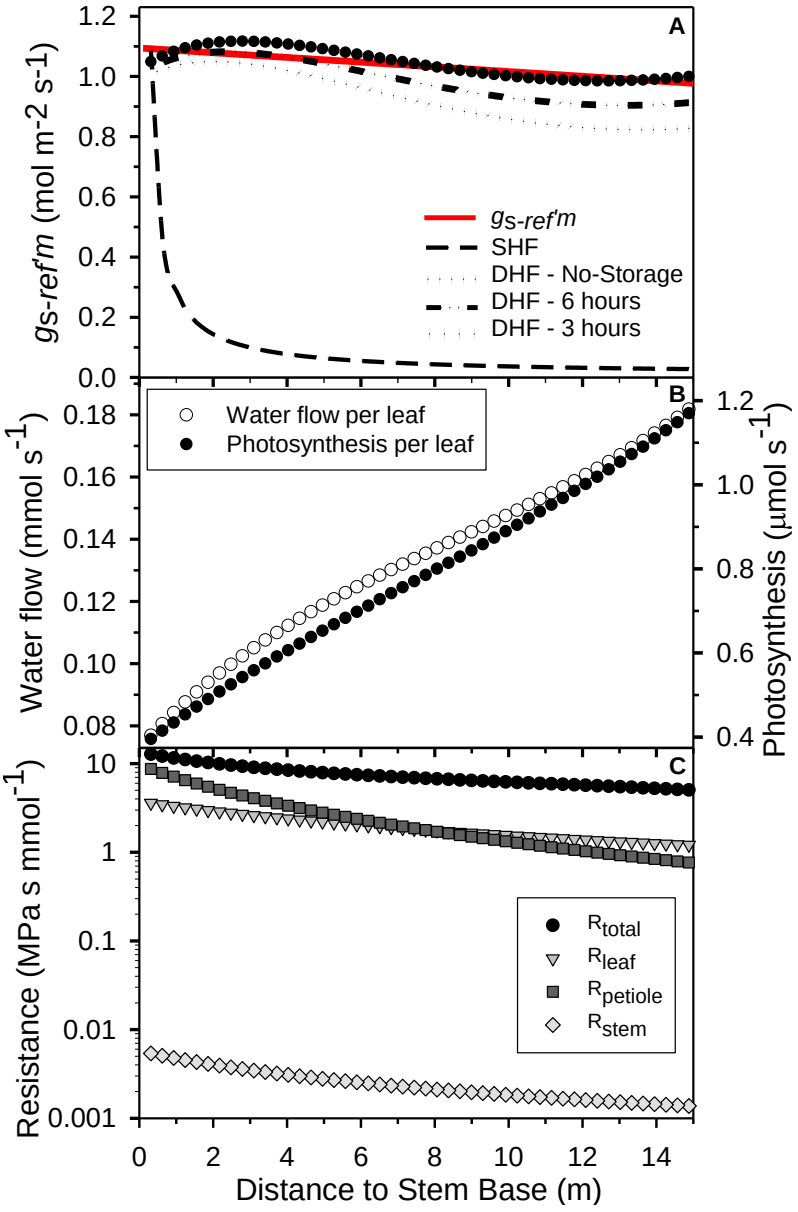

Figure 7. Modeled and measured (regression shown in red with its 95% confidence interval) decline in kudzu maximum reference stomatal conductance ($g_{s\text{-}ref}'m$) indicated an appreciable role of water storage. **A**. Predicted decline in stomatal conductance according to the simplified hydraulic formulation (SHF) and the distributed hydraulic formulation (DHF). Models were run using regressions of data (Figs. 4-6), with internode length set to 30 cm. Even though kudzu capacitance represented only 8% and 12% of the water flux at the base and at the top of the stem, respectively, plant water storage must be considered for the model to agree with the observations. **B**. Increase in water flow and net leaf-level photosynthesis (note that those values are represented per leaf, not on a leaf-area basis) with distance to stem at modelled $g_{s\text{-}ref}'m$ (DHF model with no storage in panel A). **C**. Axial (stem) and radial (leaf and petiole) hydraulic resistances to water with distance to stem base (note the logarithmic scale) showing that lateral resistances dominated the overall vine water transport capacity. The total resistance (R_{total}) to water movement at each node is also shown and decreased from 12 to 5 MPa s mmol^{-1} from the bottom the top of the vine.

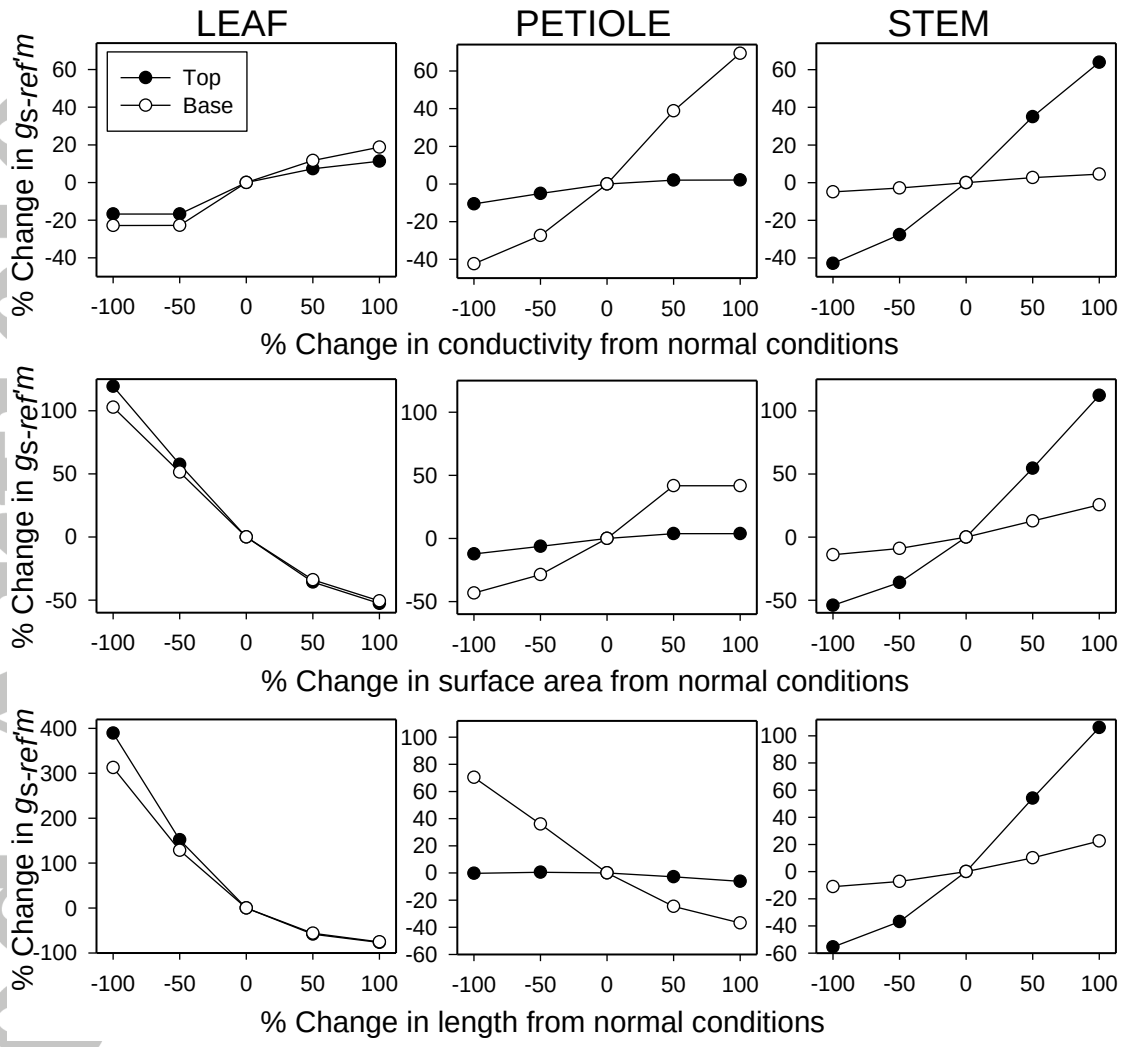

Figure 8. Analysis of the sensitivity of maximum reference stomatal conductance ($g_{s\text{-}ref}'m$) at the base and the top of the kudzu vine to changes in the values of three leaf, petiole and stem key parameters (paths length, areas, and conductivities). Each of these parameters were varied individually, with the actual magnitude of variation applied in each case reflecting the observed variability in the parameter. Axes show the percentage change in the parameters and predicted $g_{s\text{-}ref}'m$. For baseline $g_{s\text{-}ref}'m$ values and input parameters see Figure 7A and Table 4, respectively. Note for leaf length the different scales on y-axes.

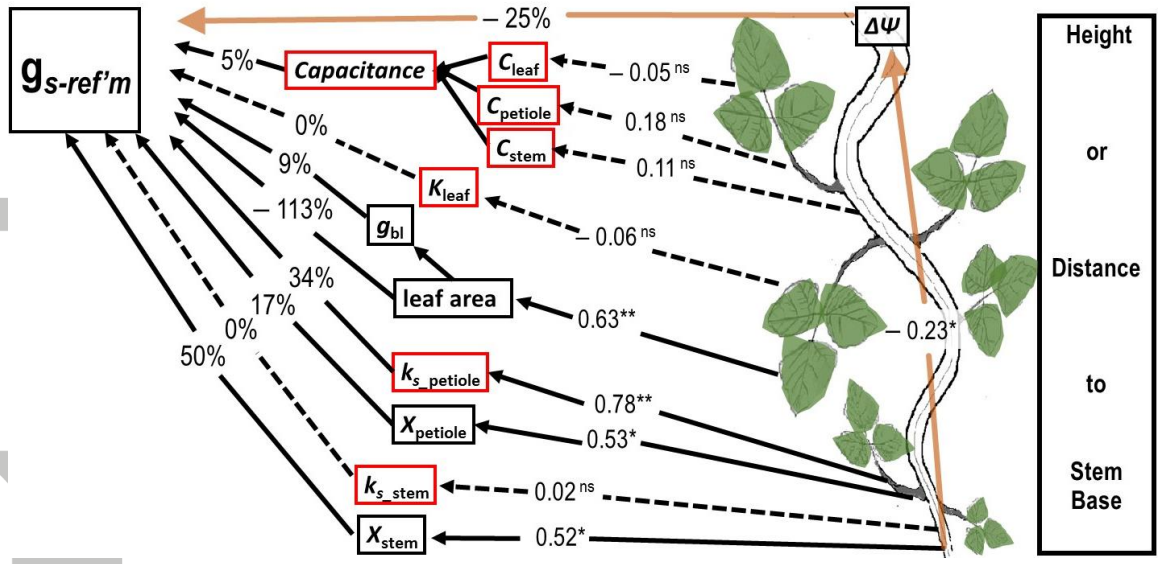

Figure 9. Conceptual diagram outlining the measured percentage height-induced changes in hydraulic (red boxes) and structural (black boxes) traits on the computed reference stomatal conductance ($g_{s\text{-}ref}'m$) predicted from the Distributed Hydraulic Formulation (DHF) model (Table 4). Regression coefficients are shown on the arrows originating from the Height/Distance to Stem Base box (ns = not significant, i.e. p> 0.05; *p < 0.05; **p < 0.01). Dotted lines indicate nonsignificant paths.